Investigating the concerted release of myosin on regulated thin filaments using single molecule microscopy.

A thesis submitted to the University of Kent for the degree of

MSc Biochemistry

2020

Quentin M. Smith

School of Biosciences

1. Declaration

No part of this thesis has been submitted in support of an application for any degree or qualification of the University of Kent or any other University or institute of learning.

Quentin M. Smith

October 2020

2. Acknowledgements

I would like to express my special thanks of gratitude to my supervisor, Dr Neil Kad, whom even before this research project has taken me under his wing and built me up into the scientist I am today. I would like to thank him for his endless support over the years, especially during this master's project, his door would always be open to help me when needed and provided his expertise to get this project going.

I would like to thank Dr Alex Moores for all her help in the lab, her expertise in molecular and microbiology is unmatched and was a big help during my masters. I would also like to give a big thank you to Dr Chloe Johnson and Dr Jonny Walklate for all their support with anything muscles related, they were voices of joy, reason and ideas when working on this project.

I would also like to thank all my colleagues from the Kad lab and the MAG lab, everyone who I have worked with which I can call friends, it was a pleasure working with you all and making this masters enjoyable - putting a smile on my face when I am working in the lab.

Finally, I would like to express my deepest gratitude to God, my family and friends who provided support every minute of the day.

3. Table of Contents

4. List of Figures and Tables

Figures:

Tables:

5. Abbreviations

Abbreviation	Definition
ABT	Actin-BSA-Tween
APTES	(3-Aminopropyl) triethoxysilane
ATP	Adenosine triphosphate
BSA	Bovine Serum Albumin
Ca^{2+}	Calcium (2+) ions
DNA	Deoxyribonucleic acid
DoG	Difference of Gaussian
EDTA	Ethylenediaminetetraacetic acid
ELC	Essential Light Chain
GI	Gastrointestinal
Gq	G-coupled receptor
HCM	Hypertrophic Cardiomyopathy
IMAC	Immobilised Metal Affinity Chromatography
IP_3	Inositol trisphosphate
IPTG	Isopropyl β-d-1-thiogalactopyranoside
LB	Luria-Bertani
LoG	Laplacian of Gaussian
mPEG	Methoxypolyethylene glycol
MWCO	Molecular Weight Cut Off
MyBP-C	Myosin Binding Protein C
Na^{+}	Sodium (+) ions
OAF	Oblique Angle Fluorescence
PCR	Polymerase Chain Reaction
P_i	Inorganic phosphate
RJMCMC	Reversible Jump Monte Carlo Markov Chain
RLC	Regulatory Light Chain
RTF	Regulated Thin Filament
RyR	Ryanodine receptor
S1	Subfragment-1 of Myosin
SERCA	Sarco-endoplasmic reticulum Ca^{2+}-ATPase
Tm	Tropomyosin
Tn	Troponin Complex
TnC	Troponin C
TnI	Troponin I
TnT	Troponin T
TRITC	Tetramethylrhodamine
UV	Ultraviolet

6. Abstract

Contraction and force generation in muscle occurs via interactions between thick and thin filaments within the subcellular sarcomere structure of fused muscle cells (myofibrils). This heavily regulated process involves the coordinated efforts of tropomyosin, the troponin complex, myosin binding protein C and other accessory proteins. The regulation of muscle contraction is important for both contraction and relaxation, for example in the heart, the former leads to pumping and the latter refilling of the cardiac chambers. The focus of this thesis is the relaxation of muscle, which is highly relevant to diseases such as HCM. Using single molecule microscopy, the dynamics of thin filament activation have been measured in a metastable condition, between contraction and relaxation. This provides a molecular insight into both processes at the same time. Here I have developed a suite of analysis programs to investigate how the muscle regulatory system relaxes. Analysis of events has revealed that myosin molecules attached to regulated thin filaments are released in a concerted fashion, a process we call catastrophic collapse. With this understanding and new analytical tools, we are now in a position to analyse mutations associated with HCM to shed light on how these affect the relaxation dynamics of thin filaments in disease.

7. Introduction

7.1. The Muscular System

7.1.1. Muscle Types

Muscle is found throughout the various motile and non-motile systems in every animal, ranging in purpose from enabling digestion, enabling gross movements and pumping blood. Its ubiquitous presence in organisms illustrates its physiological importance but also provides reasoning for its high conservation (Ng *et al.*, 1985), for example, actin is considered as a universal polymerisation machine (Gunning *et al.*, 2015a) and in higher vertebrates the proteins share a ≥ 94% sequence identity (Zhu *et al.*, 2013; Vedula and Kashina, 2018).

Depending on role, three types of muscle exist: skeletal, cardiac, and smooth. At a glance, the arrangement of each sarcomere seems similar, however, their location within the body and the addition of accessory proteins differs between them and ultimately determines their contractile function (Sweeney and Hammers, 2018). Skeletal muscle is a voluntary muscle that attaches to bones via tendons, it is the muscle group that coordinates the movement of your body. Each muscle cell (myocyte) is multinucleated and has a striated appearance due to the highly organised pattern of proteins sarcomeres (discussed later). The second muscle type, cardiac, is found solely in the heart and each cardiomyocyte must work in a synchronised fashion to coordinate continuous contraction. Finally, smooth muscle contracts involuntarily, serving many functions involving visceral organs such as digestion in your intestines, gastrointestinal (GI) tract (peristalsis) and regulation of blood pressure. Within a myocyte there are thousands of sarcomeres working in a synchronised fashion to contract and relax due to the presence of Ca^{2+} ions and the phosphorylation of the regulatory and essential light chains on muscle myosin II (Dillon *et al.*, 1981; Hai and Murphy, 1989).

7.1.2. Muscle Contraction

Muscle contraction is dependent on the subtype of muscle within the body. The mechanism differs between striated muscle and smooth muscle.

Striated muscle has contraction due to excitation-contraction coupling (Kuo and Ehrlich, 2015). This is where neurotransmitters depolarise membranes, influencing receptors to increase local calcium concentrations which ultimately leads to contraction of the muscle. These neurotransmitters bind to receptors on the motor end plate and causes an influx of sodium (Na^{+}) ions which depolarises the membrane across the surface of the muscle tissue and depolarises the T-tubule system. The depolarisation of the T-tubules triggers a shift in the resting membrane potential of the muscle, and it turns on the voltage gated channels causing further depolarisation. This causes a stimulation of L-type calcium channels which opens Ryanodine Receptor (RyR) 1 or Ryanodine Receptor (RyR) 2 channels to release of calcium (Ca^{2+}) ions from the sarcoplasmic reticulum to activate the skeletal or cardiac muscle, respectively (Bootman, 2012). Ultimately this influx of Ca^{2+} leads to interactions with troponin C allowing conformational change of the tropomyosin and in turn exposing

the myosin binding sites on actin for the myosin heads so that activation of thin filament can occur.

Smooth muscle receives its excitation via the autonomous nervous system which leads to an intracellular calcium influx which causes contraction of the muscle. This is similar to striated muscle where depolarisation causes activation of L-type calcium channels which leads to an increase in intracellular calcium and thus contraction of muscle. However, there is another pathway that is responsible for muscle contraction, which involves the activation of G-coupled (Gq) receptors which leads to the production of inositol 1,4,5-triphosphate (IP_3) which is made by the protein phospholipase C. IP_3 is an ubiquitous secondary messenger which can open IP_3 receptors on the surface of the sarcoplasmic reticulum. This in turn causes an increase in intracellular calcium which is the driving force for muscle contraction (Bezprozvanny *et al.*, 1991; Finch *et al.*, 1991).

7.1.3. Sliding Filament Theory

This description of muscle contraction dates back to 1954 where two studies by A. F. Huxley and R. Niedergerke and H. E. Huxley and J. Hanson describe the process of muscle contraction visualised via high resolution microscopy (Huxley and Niedergerke, 1954; Huxley and Hanson, 1954). In the former study, they initially show the striated pattern of the muscle tissue is what we now know to be the ultrastructure of thick and thin filaments. This allowed measurements of the sarcomere length to be made before and after isotonic contractions (Huxley and Niedergerke, 1954). These measurements allow the differences to be highlighted in the band sizes e.g. I-bands become narrower during contraction. The second study outlines the changes in the cross striations during contraction and stretching of the muscle, various conditions were applied, for example, using concentrated vs dilute ATP or controlling shortening by holding both ends of the muscle fibre (Huxley and Hanson, 1954). These studies were done via light microscopy and verified by electron microscopy and similar results were also seen via X-ray diffraction studies (Hanson and Huxley, 1953).

Essentially, this theory suggests a simple model that describes the changes of the cross striations during muscle contraction. It states that in the sarcomere there are two bands, where the I band contains non-overlapping actin filaments and the A band contain myosin and both non and the overlap region. During contraction, the I band shortens, and the A band remains constant, so visually the I band slides over the A band, hence the sliding filament model.

7.1.4. Three-state model of thin filament activation

The three-state model of thin filament activation (Maytum *et al.*, 1999) describes the propensity of myosin to form an actomyosin complex. These affinities directly correspond to the positioning of tropomyosin. The positioning of tropomyosin is influenced by troponin sensing an influx in local calcium levels. This model states that the three states of activation are the following: blocked, closed and open. Where, the blocked state involves tropomyosin completely blocking all the myosin binding sites along thin filament. The closed state is where there is an increased level of calcium which is sensed by troponin allowing tropomyosin to move more freely. The open state is where myosin has a high

affinity. This is where all the components of the muscular system are present and working together so that myosin can bind strongly to actin whilst tropomyosin shifts to allow lateral activation of thin filament as illustrated in Figure 1.

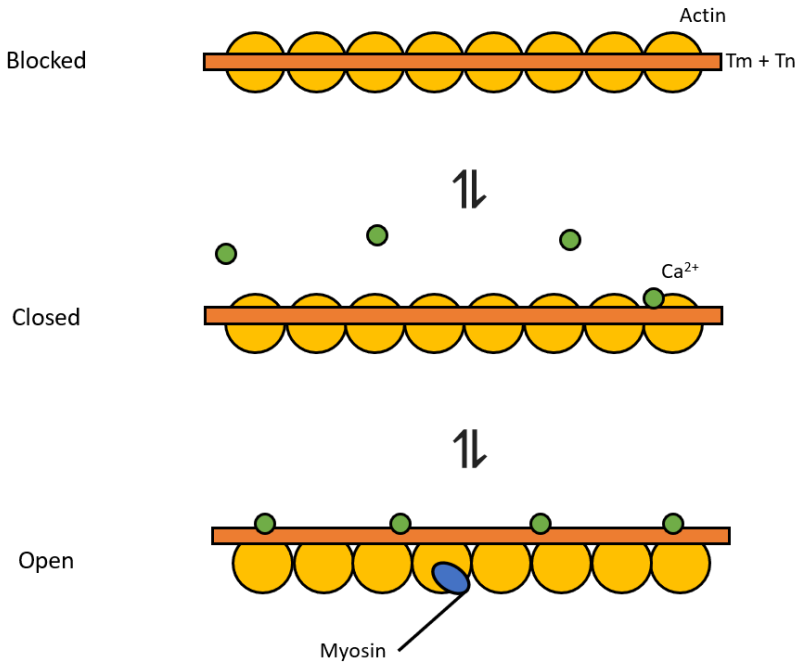

Figure 1 - The three-state model of thin filament activation.

Illustrating two transitions between the blocked and closed states and the closed and open states. The blocked state shows tropomyosin completely covering myosin binding sites located on actin, there are no other components of the muscular system that are present such as calcium, myosin and ATP. The blocked and closed states are in equilibrium and in the presence of Ca^{2+} ions, the blocked state can transition to the closed state, where calcium can activate the troponin complex allowing flexibility of tropomyosin, exposing the myosin binding sites. It is where the addition of ATP and myosin can cause the transition from the closed state to the open state where myosin can bind to the myosin binding site located on actin and induce thin filament activation. Illustration is not to scale as myosin motor domain is 130 kDa and each actin monomer is 42 kDa.

7.1.5. Force Generation

The interactions between actin and myosin in the presence of calcium and ATP generate force and motion. This motion generated is from a process called the crossbridge cycle which was derived from the Lymn-Taylor cycle (Lymn and Taylor, 1971). The crossbridge cycle consists of four steps. The first step consists of crossbridge formation, whereby the activated myosin can bind to actin to form a stable actomyosin complex. Myosin is activated by ATP binding to the ATPase site on the myosin head so that ATP can be hydrolysed into ADP and inorganic phosphate (P_i). The next step is where the hydrolysis of ATP leads to ADP and inorganic phosphate to be released causing a power-stroke to occur allowing myosin to create a rowing like movement across the actin (Holmes, 1997; Geeves and Holmes, 1999). Now that the ATPase site on myosin is free, local ATP is able to rebind to that site and causes the myosin from the crossbridge to detach from the actin. Finally, reactivation of the myosin head must occur via the hydrolysis of ATP to complete the

crossbridge cycle, this is illustrated in Figure 2. The forces generated from this crossbridge cycle have been extensively studied over the years via *in vitro* motility assays (Homsher *et al.*, 1996; Greenberg and Moore, 2010), X-ray diffraction studies (Irving *et al.*, 1992) and force-tension experiments (Karatzaferi *et al.*, 2004).

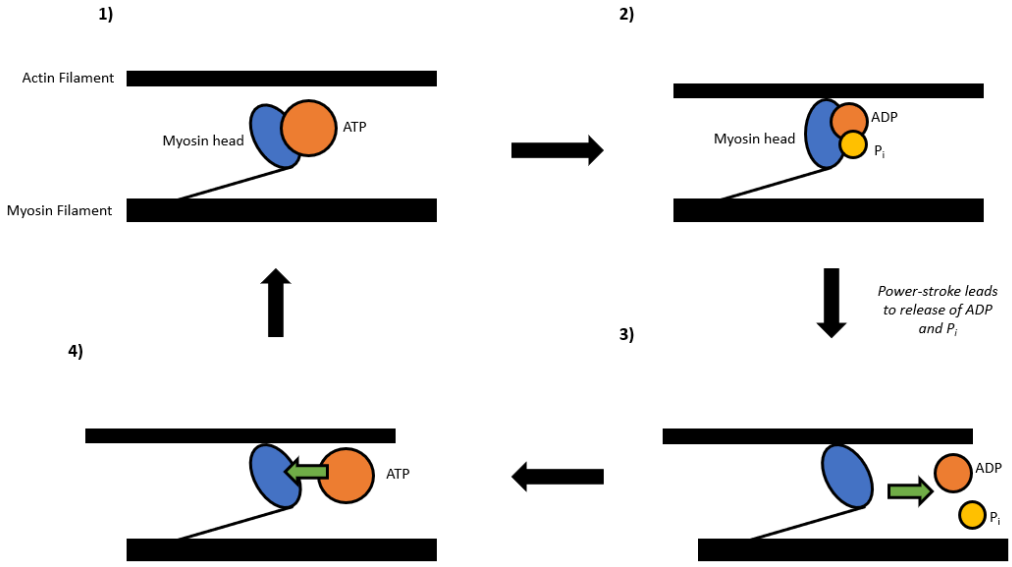

Figure 2 - The crossbridge model of muscular contraction, illustrating the hydrolysis of ATP.

This schematic (not to scale) illustrates the crossbridge cycle in muscular contraction. Where 1) shows ATP binding to the myosin head, whereby in 2) hydrolysis of ATP activates the myosin head allowing a crossbridge to form, but as ADP and P_i are released, a power stroke occurs – this is seen in 3) where the myosin head has a change in angle thus moving actin filament along. Finally, in 4) the myosin head is reactivated in the presence of ATP.

7.2. The Sarcomere

7.2.1. Structure & Function

The sarcomere is the smallest contractile unit within muscle. This repeating arrangement of thick and thin filament allows a length-tension relationship that is responsible for muscular contraction (Au, 2004). In its most relaxed state, force tension experiments have shown the sarcomere to be a length of 2.4 µm (Johnston *et al.*, 2016). These experiments play on the structure of the sarcomere and highlight the function of each component. Initially they show that ATP hydrolysis is done by the thick filament, thin filament is activated by Ca^{2+} and other regulatory proteins such as Myosin Binding Protein C, Tropomyosin, and the Troponin Complex interact with each other at varying degrees and contribute to the regulation of muscular contraction. More recent studies shows that MyBP-C governs interactions with both thick and thin filament (Heling *et al.*, 2020) and tropomyosin along with the troponin complex has various degrees of interactions with thick and thin filament also, this will be described later.

7.2.2. Calcium role of regulation of contraction

Every muscle requires calcium for contraction, it is the main signalling molecule which controls contraction and relaxation of the different muscle types, in the absence of calcium there is no interaction between actin and myosin (Szent-Györgyi, 1975). Calcium is released due to a change in stimuli which is caused by neurotransmitter release which in turn interacts with receptors to release stores of calcium in the sarcoplasmic reticulum. Depending on the tissue type as described earlier, calcium can interact in different ways such as directly associating with Troponin C and causing conformational change in tropomyosin, or calcium can interact with G-coupled receptors and release IP_3 which causes even more of an influx of calcium which then can activate myosin light-chain kinase to initiate muscle contraction (Berchtold *et al.*, 2000).

To regulate Ca^{2+} homeostasis, calcium is pumped back from the cytosol of the myocyte into the sarcoplasmic reticulum via the sarco-endoplasmic reticulum Ca^{2+}-ATPase (SERCA) so that the muscle can relax (Periasamy *et al.*, 2008) and be ready for another potential activation.

7.3. Thin Filament

7.3.1. Actin

Actin was discovered and successfully isolated by Straub in 1942 from myosin which usually is in a complex called actomyosin. The 42-kDa protein monomer forms polar, double stranded helical filaments (F-actin). Actin has many purposes in eukaryotic organisms (Dominguez and Holmes, 2011) however, more specifically in muscle, its purpose is to allow muscle contraction via its interactions with myosin and accessory proteins. The filament has two ends, termed barbed and pointed and they represent what side is more active in terms of elongation, studies have shown that the pointed end is more active in its rate of elongation and leads to actin treadmilling (Wegner and Isenberg, 1983). X-ray crystallography and electron microscopy studies have shown the detail in structure of F-actin, and it does confirm its two chained right-handed helix conformation(Dominguez and Holmes, 2011).

Actin has ATPase activity which is required during filament assembly and allows the cross-bridge cycle to occur when an interaction between myosin has been made. In the cross-bridge cycle, as myosin binds to actin in the presence of ATP, ATP is then hydrolysed into ADP whilst releasing inorganic phosphate. This causes a conformational change in myosin allowing it to generate force for the power stroke and ultimately moves actin along towards the M-line (the middle of the sarcomere) during contraction.

7.3.2. Tropomyosin

Tropomyosin, discovered in 1946 by Kenneth Bailey is a long 65 kDa protein dimer which has two alpha helices (32.5 kDa each) which are wound in a rigid coiled coil orientation (Bailey, 1946). It forms head to tail polar filaments alongside the thin filament (Gunning *et al.*, 2015b). Tropomyosin has two striated muscle isoforms (α and β) which polymerise in low ionic strength solutions (Ooi *et al.*, 1962; Paulucci *et al.*, 2004). It polymerises along the major groove of actin filaments and correct spacing of the homodimer αβ complex allows for cooperative activation of thin filament (Hitchcock-DeGregori and An, 1996; Schevzov *et al.*, 2012).

The shape and conformation of tropomyosin has the primary roles of stabilising thin filament and regulating muscle contraction via steric hinderance. Tropomyosin has a strong affinity to the thin filament and it has been confirmed via deletion studies (Hitchcock-DeGregori *et al.*, 2001), the highly conserved N-terminal half of tropomyosin's period 5 is home to the internal region responsible for this (Brown *et al.*, 2005)·(Hitchcock-DeGregori and Singh, 2010).

Studies have shown that tropomyosin has two states, essentially "on" and "off" which is influenced by the presence of troponin which leads to the cooperative binding of S1 (Geeves and Lehrer, 1994). Tropomyosin has interactions with the C-terminal domain of TnI which causes displacement of tropomyosin and allows myosin interaction with actin (Galińska-Rakoczy *et al.*, 2008; Lehman *et al.*, 2009).

7.3.3. Troponin Complex

Troponin was discovered in 1963 by Setsuro Ebashi which led to the investigation of calcium regulation during muscular contraction. The troponin complex is a large multi subunit complex with a size of about 80 kDa (Ohtsuki and Morimoto, 2013). Each subunit of troponin: Troponin I (TnI), Troponin C (TnC) and Troponin T (TnT), has a different structure and function and studies have now shown the structure and function of each component of the troponin complex using X-ray crystallography (Takeda, 2005). Each troponin subunit alongside tropomyosin allows the inhibition of contraction of thin filament.

Troponin I is a globular protein around 37 kDa (cardiac molecular weight (Dasgupta and Wahed, 2014)) and has been classed as the inhibitory subunit of the complex, as it inhibits the actin-myosin interaction (Perry, 1999; Geeves, 2012). TnI has multiple functions such as inhibiting myosin binding to actin, inhibiting actomyosin ATPase and reversal of inhibition by activation of TnC (Geeves *et al.*, 2000; Ohtsuki and Morimoto, 2013).

Troponin C is a small globular protein from the calmodulin family that is around 18 kDa in size. It has the role of binding to Ca^{2+} ions and interacting with troponin I to stop its inhibitory effects in the presence of Ca^{2+}. Skeletal troponin C has four binding sites from I – IV and they have varying affinities to Ca^{2+}, whereby I-II have low affinities so that it can respond to larger changes in Ca^{2+} concentrations during muscle contraction and III-IV have higher affinities to Ca^{2+} which mean they are always active due to physiological ionic conditions (Herzberg *et al.*, 1987).

Troponin T has the role of binding to tropomyosin and anchoring troponin I and C subunits to the thin filament (Marques and de Oliveira, 2016). As the organiser of the complex, around 31-36 kDa and 18 nm in diameter (Tobacman, 1996; Perry, 1998) it interacts with tropomyosin and orchestrates the inhibitory function of the complex. Troponin T interacts physiologically to the I and C subunits and causes an effect on calcium sensitivity of the actomyosin MgATPase. Ultimately, the troponin complex hand in hand with tropomyosin has the regulatory role of muscle contraction.

7.4. Thick Filament

The myofilament contains the primary motors that drive muscle contraction – these motors are thick filament. Thick filament within the sarcomere is also known as muscle myosin II with a motor domain (about20 nm long) and an alpha helical coiled myosin rod (150 nm long). Alongside the core head, neck, and tail structure of myosin, within the neck region of muscle myosin II there are other components such as the essential light chain and regulatory light chain, these are the calcium sensing components of thick filament (Fusi *et al.*, 2016). Thick filament has a very organised repeating structure whereby every 43 nm along the filament there are three pairs of myosin heads around the myosin circumference, this is termed a quasi-helical organisation (Irving, 2017). Regulation of thick filament is done by the accessory protein – Myosin Binding Protein C (MyBP-C), which packs itself alongside the 9 myosins in the 43 nm repeating pattern allowing its C-terminal domain to interact with the N-terminal domain of myosin (Ratti *et al.*, 2011; Wang *et al.*, 2016; Heling *et al.*, 2020).

Thick and thin filament in the presence of Ca^{2+} expose myosin binding sites located on the thin filament and in turn cause thick filament to bind and hydrolyse ATP to cause a cross-bridge cycle. The interactions between these two work under a cooperative fashion and the generation of force from these interactions are dependent on many factors.

7.5. Project Outline

The activation of thin filament has been studied extensively over the years and more recently, single molecule studies have shown the cooperative activation of thin filament (Desai *et al.*, 2015; Longyear *et al.*, 2017; Inchingolo *et al.*, 2019). It is hypothesised that this activation is a cooperative process, whereby two myosin heads are required to laterally activate thin filament (Desai *et al.*, 2015). This hypothesis falls in line with the current three state model (McKillop and Geeves, 1993), ensemble kinetics (Maytum *et al.*, 1999) and structural studies (Vibert *et al.*, 1997). However, this is not the only component of the muscular system, relaxation is the second and equally necessary part to muscular contraction and shouldn't merely be seen as a passive process (Biesiadecki *et al.*, 2014).

Previous studies have indicated that there may be a phenomenon termed catastrophic collapse (Desai *et al.*, 2015; Inchingolo *et al.*, 2018), whereby relaxation of thin filament is not only seen as a stochastic process, but more concerted events of thin filament deactivation occur. By using the single molecule tightrope assay we are able to visualise

these events and to interpret them, statistical validation has been done via the Reversible Jump Markov Chain Monte Carlo (RJMCMC) model (Inchingolo *et al.*, 2018). To simplify the data analysis so that it is more applicable to wider data sets, I have developed a new analysis protocol to confirm the presence of catastrophic collapse. Using this analysis, we are able to hypothesise that the concerted release of myosin is an active, coordinated process which provides complete relaxation of muscle. Studies have shown impairment of muscular relaxation in diseases such as hypertrophic cardiomyopathy (HCM) (Tardiff, 2005; Li *et al.*, 2012), HCM is a common phenotype for these molecular insults and we believe this process could provide a molecular explanation for it.

My project aims are as follows:

1. To be able to extract and purify actin and muscle myosin II from *Chicken Pectoralis*
2. To be able to fluorescently label and purify S1 myosin mNeonGreen
3. To conduct single molecule fluorescent microscopy of regulated thin filament
4. Develop a new workflow for data analysis to track the catastrophic collapse of myosin clusters on regulated thin filament

8. Experimental Methods

8.1. Extraction and Purification of Myosin

8.1.1. Extraction of Muscle Myosin II from *Chicken Pectoralis*

Myosin was prepared from chicken pectoralis. Pectoralis tissue was sourced from the local butchers in the morning, excess tendons, fats and other tissue were removed, and it was rinsed with 0.2 M EDTA. The tissue was cut into small pieces and then went through the meat grinder. After this was done, 2 ml of buffer A was added per g of tissue and it was stirred gently (to avoid air bubbles) with an overhead stirrer for 12 minutes precisely. This reaction was stopped by adding cold ddH_2O up to 2 L. This 2L solution was filtered through four layers of cheesecloth and the solution was retained in a 5 L beaker. Cold ddH_2O was added to 5 L and gently stirred to solubilise – then the stir bar was removed so that the myosin could then precipitate after 3 hours in the cold room. The remaining pulp was used for the actin acetone powder preparation. The supernatant was carefully siphoned off (Stage 1 in figure 8) and the precipitate was then centrifuged at 7800 rpm (10,750 x g) in a Beckman Coulter JA-10 at 4^{o}C for 10 minutes. The supernatant was discarded (Stage 2 in figure 8), the pellet from this centrifugation step was then resuspended in 15 ml of buffer B (Stage 3 in figure 8) and dialysed overnight against 4 L of buffer C at 4^{o}C.

Day 2 involved adding equal amounts of ddH_2O to the dialysed solution in a tared beaker. This was gently stirred for 30 minutes to precipitate the actomyosin (Stage 4 – supernatant & Stage 5 – precipitate in figure 8). This solution was put in an ultracentrifuge at 20,000 rpm (41,171 x g) in a Beckman Coulter JA-25.50 rotor at 4^{o}C for 1 hour (Stage 6 – supernatant & Stage 7 – precipitate in figure 8). The pellet from this was discarded and the supernatant from this was poured into 1L beakers and diluted 10-fold with ddH_2O, it was left to set for 3 hours. The supernatant was carefully siphoned off (Stage 8 in figure 8) and the precipitate was centrifuged at 7800 rpm (10,750 x g) in a Beckman Coulter JA-10 rotor at 4^{o}C for 15 minutes. The supernatant from this centrifugation was discarded and the

pellet was homogenised (Stage 9 in figure 8) in the least amount of buffer D as possible (≤10 ml). This resuspended solution was dialysed overnight against 2L of buffer E, and it was changed the next morning and dialysed again for an additional 2 hours.

Day 3 involved clarification of myosin, spinning the dialysed solution at 20,000 rpm (41,171 G) at 4°C for 2 hours in a Beckman Coulter JA-25.50 rotor. The myosin was carefully removed from the tubing, avoiding the upper fat layer (Stage 10 – supernatant & Stage 11 – precipitate in figure 8). To determine the concentration and check the purity of the myosin from this extraction, it underwent SDS-PAGE gels and spectrophotometry at 280 nm and 320 nm (to check for myosin and its purity respectively – see table 1) at several dilutions (1:25, 1:50 and 1:100). Finally, the myosin produced is stored in 50% glycerol at 4°C.

$$\frac{mg}{ml} = \frac{(A280 - 1.7(A320))}{0.55} \times dilution\ factor$$

$$M = \frac{mg/ml}{493{,}000\ Da}$$

Table 1 - Spectrophotometry values to determine the concentration of myosin.

Serial dilutions were made, allowing three sets of values to average. The absorbances were measured at 280 nm and 320 nm, using 0.55 as an extinction coefficient for myosin, this allowed for the concentration of myosin in mg/ml and as a molarity.

Dilution	Abs_{280}	Abs_{320}	mg/ml	µM
1:25	0.341	0.93	8.3	16
1:50	0.191	0.051	9.5	19
1:100	0.107	0.026	11.4	23
Average	-	-	**9.7**	**19.3**

Table 2 - Buffers and compositions for purification of muscle myosin II from chicken pectoralis.

Buffer	Composition
A	150 mM Potassium Phosphate pH 6.7, 300 mM KCl, 20 mM EDTA, 5 mM $MgCl_2$, 5 mM DTT, 4 mM ATP
B	60 mM Potassium Phosphate pH 6.7, 1 M KCl, 20 mM EDTA, 5 mM DTT
C	25 mM Potassium Phosphate pH 6.7, 600 mM KCl, 5 mM DTT
D	50 mM Potassium Phosphate pH 6.7, 3 M KCl, 5 mM DTT
E	50 mM Potassium Phosphate pH 7, 600 mM KCl, 5 mM DTT

8.1.2. Papain digest of Myosin Head

Papain is a proteolytic enzyme derived from papaya that was used to digest full length myosin into S1 myosin, whilst retaining the regulatory light chain (RLC) and essential light chain (ELC). First, myosin had to undergo deglycerination, this was done according to this protocol (Margossian and Lowey, 1982). Dialysis of 30 mg of glycerinated myosin in 12-14 kDa dialysis tubing was done overnight against 1L of solution A (200 mM ammonium acetate, 2 mM $MgCl_2$, 1 mM DTT, pH 7.2). An extra step of dialysis was done the following morning with fresh solution A for 2 hours. The myosin suspension has increased in viscosity and now it is brought to room temperature. Solution B (1 mg/ml papain, 5 mM Cysteine, 3 mM EDTA, pH 6.0) is added (70 µl/ml) to make a final papain concentration of 0.07 mg/ml and it was immediately put on a rotating mixer and timed for 10 minutes whilst samples were taken at the start and every 5 minutes to provide a time-course gel (see Figure 9). To stop the reaction, solution C (100 mM Iodoacetic Acid) was added (50 µl/ml) to reach a final iodoacetic acid concentration of 5 mM. This digested suspension was spun down at 10,000 x g for 30 minutes at 4°C and the supernatant should solely be S1 myosin at a yield of 40% of the theoretical value. The supernatant was then purified further by using a HiTrap DEAE FF 5 ml column (GE Healthcare) which allowed purification over a 0 KCl to 250 mM salt gradient in a 50 mM Tris-HCl buffer at pH 8. SDS-PAGE gels (see Figure 9) were done to decide which fractions to pool together, and they were stored in 50% glycerol at -20°C or used in an exchange reaction.

8.2. Preparation of Thin filament

8.2.1. Preparation of Actin

Following the myosin preparation, preparation of acetone powder is done. The pulp from the myosin preparation is extracted using 50 mM $NaHCO_3$ for 12 minutes using an overhead stirrer on a speed which does not create bubbles. It is then filtered using four layers of cheesecloth after the extraction and this is done twice. Extraction is repeated again but with ddH_2O instead of $NaHCO_3$, but the extraction time is shortened to 5 minutes. Moving to a fume hood, the extraction process is done with 100% acetone for 10 minutes and this is repeated three times until the pulp has turned into somewhat of a damp powder. This powder is left on lightly covered tin foil to air-dry overnight. The following morning, the powder is weighed and stored in a conical tube in the freezer at -20°C.

Isolation of actin is done over a 4-day process. Day 1 consists of extraction of the actin using extraction buffer (Tris Base 20 mM, $CaCl_2$ 0.2 mM, 0.2 mM ATP, 1 mM DTT) on ice using an overhead stirrer for 30 minutes (again, on a speed which does not create bubbles). The solution is then spun in a JA-10 rotor at 7500 rpm (10,000 x g) for 20 minutes at 4°C and then filtered through four layers of cheesecloth – the supernatant is stored on ice and then pellet re-extracted as before but for a further 10 minutes following the same centrifuging as described above. The supernatants are combined and addition of the following: 50 mM KCl, 2 mM $MgCl_2$ and 1 mM ATP are added to polymerise the actin from its G monomer (globular) state to its F – filamentous state. Using a stir rod to gently mix the solution together it is then left for 2 hours at 4°C and an increase of viscosity should be seen. A high salt wash is done by increasing the KCl concentration from 50 mM to 600 mM using solid KCl, using a stir bar to gently mix, the solution is mixed for 30 minutes at 4°C,

this is to remove tropomyosin. After this, sedimentation of filamentous actin was done by spinning it in a Type 45 Ti rotor at 42,400 rpm (209,000 x g) for 1 hour at 4°C, the supernatant is removed and then depolymerisation is started. Depolymerisation is done by gently scraping the pellet off the tube and homogenising it with 3 ml of cold buffer A per gram of acetone powder originally extracted. Once successfully homogenised, it is dialysed against 1 L of cold extraction buffer for 1 hour at 4°C and then it is transferred to some fresh cold extraction buffer to be dialysed overnight at 4°C.

Day 2 consists of solely dialysis, whereby you change the dialysis buffer in the morning and repeat this every 8 hours in preparation for Day 3. Day 3 is where you clarify G-actin by spinning the dialysed solution in a Type 45 Ti rotor at 42,400 rpm (209,000 x g) for 1 hour at 4°C. The supernatant is then removed into a small beaker and polymerisation is done by adding 1 M imidazole and 25 mM $MgCl_2$, this is gently mixed before dialysing this solution in 2 L of storage buffer (4 mM imidazole, 0.1 M KCl, 2 mM $MgCl_2$, 1 mM DTT, pH 7) overnight at 4°C. Day 4 consists of quantifying the concentration and purity of the actin by running SDS-PAGE gels (see figure 10) and using spectrophotometric measurements at A_{280} (protein) and A_{320} (purity).

8.2.2. Preparation of Accessory Proteins

Plasmids containing rabbit α-Tropomyosin and human cardiac troponin complex were kindly donated by Professor Mike Geeves. They were transformed into E.*coli* BL21(DE3) strain, expressed and purified by Dr Alessio Inchingolo, these were stored in 3% sucrose, flash frozen and stored in the freezer at -80°C at a concentration of 110 µM and 10 µM, respectively.

8.3. *In vitro* motility assay

8.3.1. Flow chamber design

The flow chamber consists of glass slides (ThermoSci), double sided sticky tape (3M) and a 22 mm x 22 mm coverslip (glass coverslip). Firstly, glass coverslips are submerged in ddH_2O and a thin opalescent film of 50 µl nitrocellulose (Sigma-Aldrich) is formed above that, the water beneath the film of nitrocellulose is drained and the glass coverslips are allowed to dry for 30 minutes before assembling the flow cell. Meanwhile, two pieces of double-sided sticky tape (3M) are placed on either side of the glass slide. Once the nitrocellulose glass coverslips are dried the flow chamber is assembled as seen in figure 3.

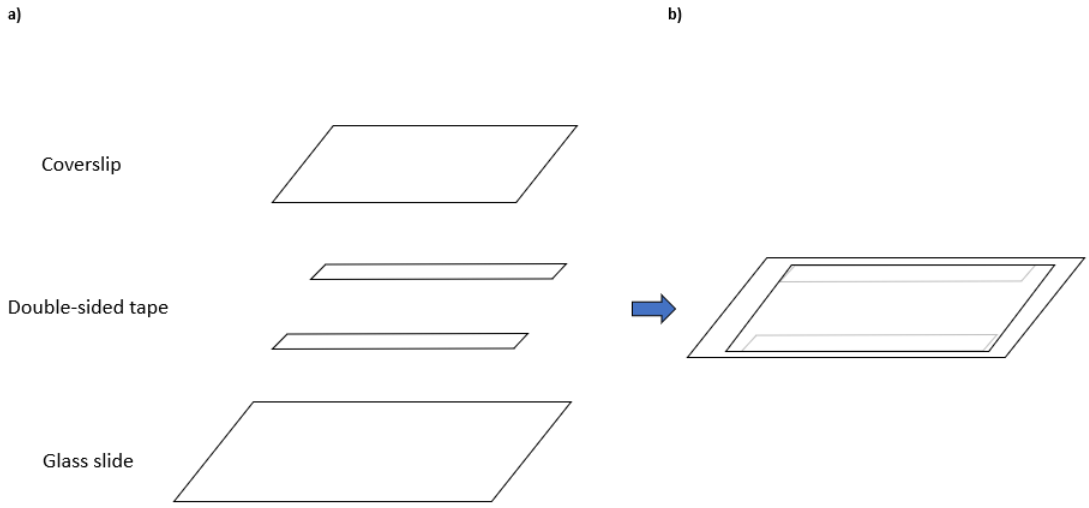

Figure 3 - Projected and assembled schematic views of a flow cell for in vitro motility assays.

a) shows the projected view of the flow cell, highlighting individual components such as glass slides, double-sided tape strips and coverslips. b) is the assembled view which is ready for incubation.

8.3.2. Incubation of flow cell for motility assay

The methods of preparing the flow cell for the motility assay were slightly adapted from (Szczesna-Cordary *et al.*, 2007; Greenberg and Moore, 2010). The following was added to the flow cell and incubated at room temperature. Firstly, 30 µl of myosin incubated for 1 minute (this was done twice), then 30 µl 0.5 mg/ml BSA (Sigma-Aldrich) incubated for 1 minute (done twice). The unlabelled actin coat was vortexed for 30 seconds to shear the actin before adding 30 µl to be incubated for 1 minute (done twice), followed by a 30 µl ATP wash (done twice) to release all actin that are attached to active myosin heads. A 30 µl 1X actin buffer wash was done twice and then TRITC-phalloidin (Sigma-Aldrich) labelled actin was very slowly pipetted and incubated for 30 seconds (slow pipetting reduced the shearing force on the actin). Another 1X actin buffer wash was done twice to remove any free moving actin and to reduce the signal to noise ratio whilst imaging. Finally, three washes of 30 µl motility buffer were done because it contains methylcellulose which causes a reduction in lateral diffusion of the actin filaments away from the surface as mentioned in (Uyeda *et al.*, 1990).

8.3.3. Single molecule fluorescent microscopy

All experiments were conducted on a custom-built oblique angle fluorescence (OAF) microscope using an Olympus IX50 inverted microscope frame. The angle of the illumination beam allows us to image the surface of the cover slip which is the pinnacle of all our surface-based imaging assays. The custom excitation path uses a 488 nm, 561 nm or 637 nm lasers which passes through an Olympus 1.45NA 100x objective lens. Dependent on the Phalloidin based dye used determined what laser would be used for each experiment.

Previously described in (Springall *et al.*, 2016), we are able to obtain triple colour images by using an Optosplit III (Carin Research, UK). Images were recorded using the Hamamatsu Orca Flash4.0 V2 with a 1x1 or 2x2 bin resulting to a 63.2 nm or 162.4 nm camera pixel size, respectively. All images and videos were processed using Fiji.

8.4. Regulated Thin Filament tightrope assay

8.4.1. Flow chamber design

Glass slides (ThermoSci) were drilled to make two 3 mm holes using a Dremel drill with diamond drill tips at maximum speed submerged in water and in a 3D printed template holder. Drilled slides were washed by soaking them in 100% Acetone (Fisher Chemical) and 100% Ethanol (Fisher Chemical) overnight on an orbital shaker. Coverslips (ThermoSci) were added alongside the drilled slides and they were placed in a plastic beaker, addition of 200 ml of 100% acetone and 4 ml (2%) of (3-Aminopropyl) triethoxysilane (APTES) was done for the silanization process which allows the subsequent attachment of our silica beads to the surface of the flow-cell. Silanization was done for 10 minutes on an orbital shaker and it was poured off and rinsed using deionized water. Each slide and coverslip was dried with nitrogen gas and placed in a rack to be cured in the oven at 105°C for 1 hour.

Plastic tubing with a 1.15 mm internal diameter (GE Healthcare) was cut down to an appropriate size and by use of a heat gun - one end was flared out. This was done to allow the tubing to stay in place whilst adding UV adhesive. UV adhesive was applied to seal the tubing to the glass slide. This was placed under a UV lamp for 2 minutes, so the adhesive fully dried, the flared-out end of the tubing was cut down using a scalpel to make what will be the inside of the flow cell. A double-sided rectangle gasket was placed encompassing each hole of the flow-cell and then the coverslip was added to create a flow chamber, this is illustrated in Figure 4.

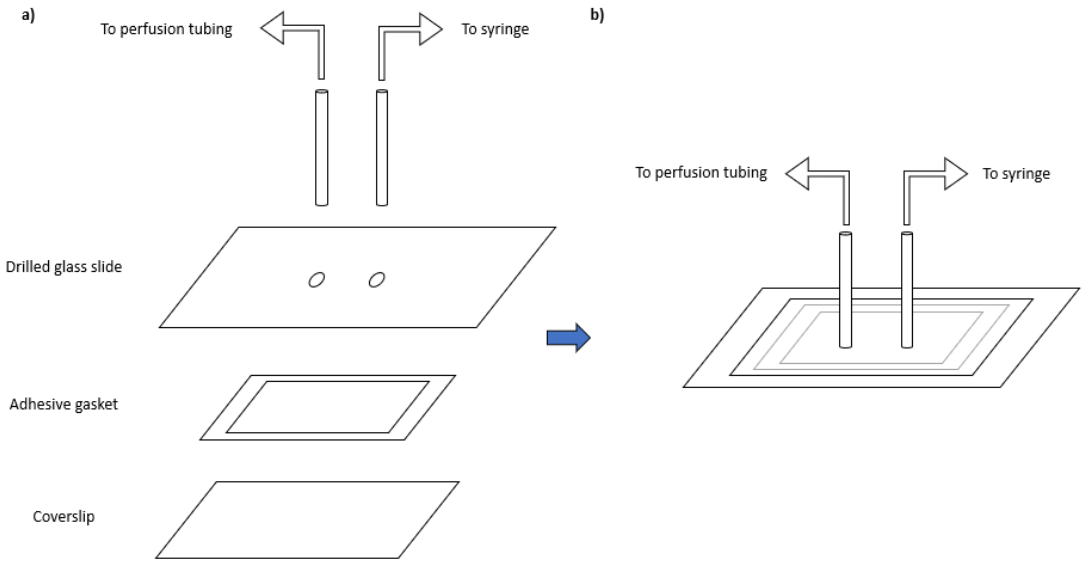

Figure 4 – Projected and assembled schematic views outlining design of a flow-cell and its connections to perfusion tubing and the syringe pump.

a) shows the projected view of a flow cell, showing individual components such as the coverslip, adhesive gasket, drilled glass slide and respective tubing. b) illustrates the assembled product of a flow-cell ready for incubation and imaging.

8.4.2. Incubation process for the flow cell

Flow cells are first washed through with 200 µl of deionised water through each port and then blocked with 80 µl of methoxypolyethylene glycol 5,000 (mPEG 5000) in proprionic acid (Sigma-Aldrich) and left overnight in the fridge at 4°C. Deionised water was then pumped through each port again to wash out any excess mPEG and then 80 µl of ABT buffer (25 mM KCl, 25 mM Imidazole, 4 mM EGTA, 4 mM $MgCl_2$, 0.1% BSA, 0.1% Tween 20,) was pumped through the flow cell and stored overnight in the fridge at 4°C. The flow cell is now ready to flow in 100 µl ddH_2O washed 5 µm silica beads (Bangs Laboratories) which adhere to the silanised coverslip.

The beads are vortexed for 15 seconds and sonicated for three 1 second pulses at 80% amplitude using a before flowing the 100 µl into the flow cell, the flow cell is checked under a Nikon light microscope for bead density to ensure there are enough beads close enough to suspend the reconstituted thin filament between. The flow cell is then washed with the calcium-based buffer (25 mM KCl, 25 mM Imidazole, 4 mM EGTA, 4 mM $MgCl_2$, 100 µM $CaCl_2$, 0.1 µM ATP, 100 mM DTT) and subsequently 500 nM of reconstituted filament is flowed through in order to suspend the RTFs on a bi-directional loop pumping back and forth at a rate of 300 µl/min for 30 minutes before loading the flow cell onto the custom-built oblique angle fluorescence (OAF) microscope.

8.4.3. Single molecule fluorescence imaging

All experiments were conducted on a custom-built oblique angle fluorescence (OAF) microscope using an Olympus IX50 inverted microscope frame. The angle of the illumination beam allows us to image the surface of the cover slip which is the pinnacle of all our surface-based imaging assays. The custom excitation path uses a 488 nm, 561 nm or 637 nm lasers which passes through an Olympus 1.45NA 100x objective lens. RTF's were labelled with a combination of Alexa Fluor 633 (Sigma-Aldrich) and Biotin-phalloidin (or phalloidin) (Sigma-Aldrich) in a 2:1:0.5 fashion being: actin, biotin-phalloidin (or phalloidin) and Alexa Fluor 633 respectively. The reasoning behind dual labelling was due to the concentration of the AF633 dye, a low concentration of 3 µM required a high volume to use to label in a typical 1:0.5 (actin:dye) fashion which ultimately led to a high amount of methanol which distorted the structure of the thin filament and made imaging single tightropes difficult.

Previously described in (Springall *et al.*, 2016), we are able to obtain triple colour images by using an Optosplit III (Carin Research, UK). Images were recorded using the Hamamatsu Orca Flash4.0 V2 with a 1x1 or 2x2 bin resulting to a 63.2 nm or 162.4 nm camera pixel size, respectively. All images and videos were processed using Fiji.

8.5. Fluorescent labelling of S1 myosin with mNeonGreen

8.5.1. Designing RLC-mNeonGreen-6xHis

S1 myosin is inherently a dark protein, to visualise it under the microscope it has to be labelled with a fluorophore. In order to do this, S1 has a component termed the regulatory light chain (RLC) which can be tagged with a fluorophore and exchanged with wildtype RLC allowing us to track its binding, releasing and diffusion under our custom-built OAF microscope. Our aim was to design a construct that contains RLC, mNeonGreen as well as a His-tag (6xHis) on the end to allow for protein purification.

PCR was performed twice on previously designed constructs of RLC-mScarlet (pET21a vector) and UvrB-mNeonGreen (pET21a vector). For the RLC-mScarlet plasmid, the aim was to linearise the plasmid whilst removing the fluorophore mScarlet. For the UvrB-mNeonGreen plasmid, the aim was to solely isolate and extend mNeonGreen with complementary ends to the RLC containing vector so it can act as an insert for the Gibson Assembly later on. Once this has been done, it was checked using 1% agarose gels (120 V for 30 minutes) and then the rest of the PCR products were run on a full length 0.8% agarose gel (120 V for 1 hour) to allow for better separation of any close or unwanted bands. The desired bands from the second gel were excised and use of a DNA extraction kit (QIAgen) allowed purification of the products for Gibson assembly. The products following these processes were ran on a 1% agarose gel (120 V for 30 minutes) (Figures 14 and 15) to provide approximate quantification by using a GeneRuler 1 kb DNA ladder (Thermo Scientific).

Gibson Assembly was done using NEBuilder HiFi DNA Assembly Master Mix (NEB), this incorporated the extended mNeonGreen insert with the RLC vector. The reaction mixture was incubated at 50^{o}C for 15 minutes and following incubation, the assembled product (Figure 13) was transformed into AAEC189 competent cells on ampicillin agar plates. Colony PCR was done to check whether the insert of the fragment was successful. Meanwhile, running a full length 1% agarose gel (Figure 16) and picking a colony to grow overnight allows us to check whether the size of RLC-mNeonGreen-6xHis fragment is correct and allows us to miniprep the next day to confirm via sequencing. Sequencing was provided by Eurofins Genomics and was manually checked using Snapgene.

8.5.2. Expression and purification of RLC-mNeonGreen-6xHis

The plasmid we designed containing RLC-mNeonGreen-6xHis was transformed into BL21 (DE3) competent cells, streaked against ampicillin agar plates and incubated overnight at 37^{o}C. The plate was picked for a colony and then the colony was placed in a 1L flask of LB to grow to OD_{600} 0.4-0.6 in a shaking incubator at 37^{o}C. Once the desired OD_{600} was met, the 1L flask and the incubator was then briefly cooled down to 25^{o}C before the addition of 1 mM IPTG. The IPTG induction was done at 25^{o}C for 3 hours in a shaking incubator. Samples were taken along the way for spectrophotometer measurements and SDS-PAGE gels (Figure 18) and after 3 hours the cells were spun down in a JA-10 rotor at 4500 x g for 10 minutes at 4^{o}C. The supernatant was discarded and visually, the pellet was luminescent yellow.

The pellet was gently resuspended in lysis buffer (50 mM NaH_2PO_4, 300 mM NaCl, 10 mM Imidazole, 5 mM DTT, protease inhibitor, lysozyme, pH 8.0) then the cells are placed in an ice bath and are sonicated for 5 minutes on a 30 second on/off cycle with a 55% amplitude. The supernatant was then centrifuged in a JA-10 rotor at 4500 x g for 30 minutes and the pellet was discarded. The supernatant was then applied to a HisTrap HP 1 ml (GE Healthcare) column at a flowrate of 1 ml/min and it was eluted over a gradient of 25 fractions. SDS-PAGE gels were done to check for purity and to help decide which fractions to pool together. The RLC-mNeonGreen-6xHis was finally quantified by spectrophotometry at absorbance 506 nm and was stored in 50% glycerol at -20°C, flash frozen in smaller aliquots or used to label S1 myosin immediately.

8.5.3. Labelling of S1 with RLC-mNeonGreen-6xHis

Since purified S1 myosin and RLC-mNeonGreen-6xHis were stored in different buffers, buffer exchange was done to prepare them for an exchange reaction. Firstly, spin concentration using a 50 MWCO Vivaspin 20 (GE Healthcare) column was done to decrease the volume of our samples to about 1 ml and it was then loaded onto an equilibrated Centripure P5 gel filtration (Generon) column with an exchange buffer (50 mM Potassium Phosphate buffer, 600 mM KCl, 10 mM EDTA, 2 mM EGTA). Each step allowed quantification of the concentration using a spectrophotometer, using the extinction coefficient of mNeonGreen at 506 nm (116000 $M^{-1}\,cm^{-1}$) and S1 at 280 nm (ε_{280}=0.83 $ml \cdot mg^{-1} cm^{-1}$) (Barua *et al.*, 2012).

Exchange reactions were set up in a 1:5 molar ratios, the reaction was stopped by the addition of 15 mM $MgCl_2$ and each reaction was pooled together. Again, spin concentration was done to decrease the volume of our samples and using the Centripure P5 gel filtration column, buffer exchange was done into the low imidazole column buffer (50 mM NaH_2PO_4, 300 mM NaCl, 20 mM imidazole, pH 8) for the final purification step.

8.5.4. Purification of S1-mNeonGreen-6xHis

The use of a HisTrap HP 1 ml (GE Healthcare) column allowed the final purification step of S1-mNeonGreen-6xHis. This was done over a gradient of 20 mM imidazole to 250 mM imidazole allowing sufficient separation over the fractions. Each fraction was quantified via spectrophotometry and SDS-PAGE gels were done to help decide which fractions to pool together. Pooled fractions were aliquoted, and flash frozen at -80°C.

8.6. Data Analysis

8.6.1. Data Analysis Workflow

The RTF tightrope assay allows us to visualise the activation of regulated thin filament (RTF) at a single molecule level (Desai *et al.*, 2015). This process is very dynamic because in sub-maximal activation conditions, fluorescently labelled S1 are allowed to bind, release, and diffuse across a single RTF. Previous attempts of analysing this data revolved around using a

Reversible Jump Markov Chain Monte Carlo (RJMCMC) model to understand the concerted release of the thin filament (Inchingolo *et al.*, 2018). However, we have now decided to take different approach because by simplifying the analysis process we can interpret the data much better. The approach we have taken was to develop an analysis suite which allows an increased level of automation by running a combination of Fiji macros, Excel formulas and MATLAB scripts. The main aim of this suite (Illustrated in Figure 5) is to provide a high throughput approach to extract and analyse data we have obtained from imaging.

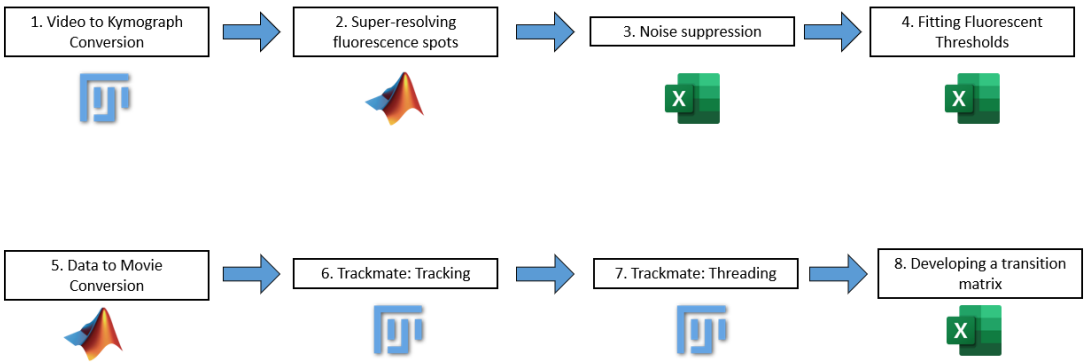

Figure 5 - Flowchart outlining each step of the new method of data analysis.

Each step of the data analysis is outlined below alongside what software accompanies it, 1) is where we convert imaging data into kymographic projections. 2) Is where we use a MATLAB script to super-resolve fluorescence spots using the 'Ezyfit' toolbox. 3) Using Excel, we are able to filter out anomalous Gaussians fits and scale up data to be used in Trackmate. 4) By fitting amplitudes to several Gaussians, we are able to create fluorescent thresholds that we can assign a number of myosin molecules to. 5) Converting the scaled-up data from the Excel spreadsheet we are able to create a scaled-up movie using a MATLAB script. 6) Trackmate is used to track the number of myosin spots there are using parameters from the Excel spreadsheet. 7) Using a simple LAP tracker, Trackmate can thread spots within predetermined displacement values. 8) Using the threaded data, we can develop a transition matrix to determine the probabilities of cluster size changes.

8.6.2. Converting Imaged Data to Kymographic Projections

Firstly, we must extract kymograph data from our imaging videos using Fiji. Whilst playing back the videos, bright spots appear to be flashing and moving along the tightrope (seen in Figure 6a), this is the active region that we are looking for. A Z-projection of the RTF is done to highlight the max intensity of the spots on the tightrope for the entire video (seen in Figure 6b), thus, allowing us to visualise the active regions. By highlighting this region, we can create a straight line through this active region and then copy it over to the original video (seen in Figure 6c and 6d). Once done, we can reslice the video and create a kymograph whilst avoiding interpolation (seen in Figure 6e). In order to get a more defined kymograph, a rolling ball background subtraction is done at 50 pixels to highlight the active regions and remove the majority of the background noise (seen in Figure 6f). Finally, this kymograph is converted into a 32-bit format preserving the intensity values and it is saved in the .tiff file format.

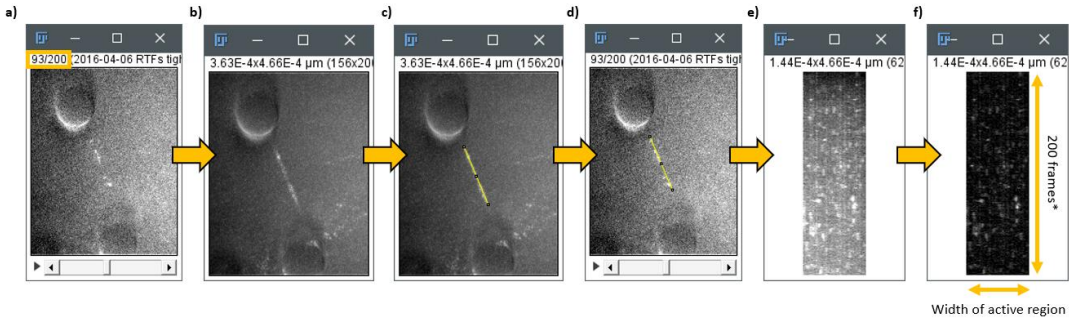

Figure 6 - Converting captured videos into kymographic projections.

a) highlights the original video captured, note on the top left of the window there are 200 frames for this video. b) a Z-projection has been done for the max intensity of fluorescent spots within the video, this shows the brightest spots and highlights our active region. c) the active region is then highlighted using a straight line to capture all the events within that region. d) copying the straight line onto the original video (Shift+E shortcut) allows us to capture the events on the video too. e) we are able to create a kymograph avoiding interpolation which shows all the binding events across the 200 frames. f) final kymographic processing consists of background subtraction using a rolling ball of 50 px and converting the image to 32-bit to conserve all intensity values.

8.6.3. Super-resolving fluorescent myosin spots

Super-resolving myosin spots is done by the second piece of the suite called 'The ring', which aims to encompass all the fitting and positional tracking of fluorescent spots on the kymograph. It is coded in MATLAB by Dr Neil Kad and allows the fitting of multiple Gaussians on each slice of the kymograph. It does this in four steps:

1. Initial Gaussian Fitting
2. Threshold filtering the Fit
3. Finding Peaks
4. Fitting Peaks

Firstly, the program allows you to choose the file of interest and then it calculates the mean positions and the max intensities of spots for each slice. Secondly, by inspecting the intensity values of the kymograph beforehand, you can apply a threshold value to ignore intensities that are below said value. For our analysis, we have determined that on average fluorescent spots have an intensity that is typically brighter than 100 a.u. and anything below is considered as background noise. Doing this allows filtering of the background noise which could be mistaken as a myosin intensity peak. After this threshold has been applied, the script looks for the number of peaks and sorts each value found in chronological order. A toolbox named 'EzyFit v2.45' is used to fit each peak to a respective Gaussian curve, the script allows up to 20 peaks to be fit simultaneously on one slice of the kymograph, but this can be increased further if necessary. After fitting the peaks, a plethora of variables will become available in the workspace of MATLAB. The variable of interest containing our data is termed 'fitline' (highlighted in Figure 7c) which we can take the values here and input it into 'The book'.

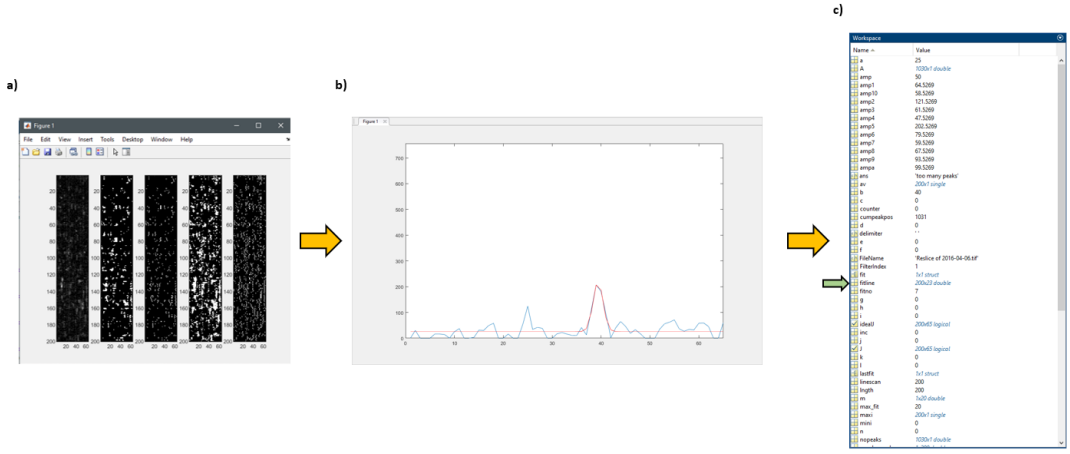

Figure 7 - Super-resolving fluorescent myosin spots using a custom MATLAB routine.

a) shows the first three steps of 'The ring', MATLAB reconstructs the kymograph several times by fitting an initial gaussian, using a threshold filter and finding precise peaks. b) is the final stage of 'The ring' whereby these peaks are fit using the 'Ezyfit' toolbox in MATLAB. c) shows the final workspace with all the parameters, the green arrow highlights our parameter of interest – 'fitline'.

8.6.4. Noise suppression

The MATLAB script uses the 'Ezyfit' toolbox and provides unbiased routine fitting which may produce some errors. This is cleaned up in the first (Main Analysis) spreadsheet by sorting, filtering and scaling up the data, allowing it to be used in Trackmate. The first spreadsheet takes the data from the 'fitline' variable and it restructures it in a columnar format, this allows correct correlation between corresponding amplitude and mean values. The amplitudes are filtered to only include Gaussians that are positively fitted (values which are greater than zero) and the means are filtered only to encompass Gaussians that are within 0 and the maximum width of the kymograph which is variable between each kymograph (for example, one kymograph can be 40 px wide x 200 px long). The initial filtering of the amplitude and means are separate, so next we combine these filters which means if we have a value in the same amplitude and corresponding mean, this value is kept, if it is one or the other, it is removed (for example, if mean 1 is present, and amplitude 1 is not, the values are not kept, both need to be present to be kept). Meanwhile, the frequency of each amplitude is calculated using COUNTIF statements and a frequency table is generated and used in the 'Amplitude Fitting' sheet. After this, rounding to 1 decimal place is done so that the raw intensity values in this data would be counted as individual pixels when imported into Fiji. Therefore, to account for sub-pixels, these positions are upscaled accordingly by a factor of 10 due to the 1 decimal place rounding, this provides us with integers and will be counted as individual pixels in Trackmate. After error removal, the final mean and amplitude values are presented at the rightmost part of the 'Main Analysis' sheet. The threshold value for Trackmate is calculated, this value is essentially the lowest mean from the data, this is calculated by using the SMALL formula in Excel. Also, the total number of spots that could be seen by Trackmate is calculated, this essentially counts the final mean values present using the COUNTIF function, however, Trackmate counts spots that move positionally, so if there is a spot that stays in the same

position over two frames, it will not be counted as a different spot, hence, when tracking in Trackmate, the value may seem less than what it actually is – this calculation solely acts as a guideline. Finally, on the 'Main Analysis' sheet, the number of spots per slice is calculated by COUNTIF functions as well, this also acts as an indicator to see if Trackmate is tracking the number of spots per slice correctly.

The next two sheets are termed 'Positioning' and 'Error Removal' respectively, as they position the mean values to the corresponding amplitude using nested IF functions, and then using the IFERROR function to remove error values which are replaced with zeros to act as blank pixels. The results from the 'Error Removal' sheet are copied to a text file which is imported into a MATLAB script described later on.

8.6.5. Fitting Fluorescent Thresholds of Individual Myosin Molecules

The next sheet on the spreadsheet is termed 'Amplitude Fitting' and this essentially takes the results from the Bin-Frequency table and fits up to 8 Gaussian curves to the raw curve (where this can be increased if necessary). It does this by calculating the sum of the Gaussians and the sum of the square differences to fit the fitted curve to the raw one that was generated, in order to get an accurate fit, Excel's solver is used. By doing this, we are able to transpose the amplitude and mean values, these mean values are considered the values that are the intensities that correspond to the number of myosins. Ultimately, we are able to make a lookup table which revolves around each myosin intensity being surrounded by 2 standard deviations to capture 95% of spots from the mean myosin intensities.

8.6.6. Converting Raw Data into a Movie

As aforementioned, the 'Error Removal' sheet contains the data we use for this stage. We copy it into a text file, this text file is imported to a MATLAB script termed 'kymograph2mov'. This MATLAB script essentially takes each slice of the data and converts into a movie with the .mj2 file format. The .mj2 file format is used to conserve the intensity values of the myosin 'spots'.

8.6.7. Tracking Fluorescent Myosin Spots using Trackmate

Trackmate is an open-source application for single particle tracking available via Fiji (version 5.0.2) (Tinevez *et al.*, 2017). Whilst Trackmate has been mainly used to track particles in a 3D space (Jaqaman *et al.*, 2008), we have decided to adjust the use of Trackmate to fit our method of analysis. We use Trackmate because previously this was a heavily manual process of threading and tracking active regions of thin filament, by using Trackmate alongside our analysis suite we are able to create a high-throughput method of analysis whilst improving the quality of the results. Trackmate offers various detectors to find and track 'spots', we've decided to use the Laplacian of Gaussian (LoG) detector

because it has proven the most accurate detector versus the other ones offered such as the Differences of Gaussian (DoG) detector. Adjustable parameters were offered by this detector, in which, we decided to choose our estimated spot diameter to be 1 pixel and the threshold to be the minimum intensity from the array of intensities from the 'Main Analysis' sheet. Meanwhile, 'median filter' and 'sub-pixel localisation' are turned off because they are not needed. There are other filter menus after the initial setup, but these were also left untouched. Using a simple LAP tracker, we are able to set several parameters such as max linking distance (pixel), max gap-closing distance (pixel) and max frame gap for gap closing which can allow threading of our 'spots'. These values are determined from the final sheet on the first spreadsheet is termed 'Average Displacement Length', this sheet essentially takes the measurements of the width of active regions on each kymograph and averages the myosin displacement and multiplies it by 10 (scaling as mentioned in section 8.6.4.) , this value is then used in Trackmate to determine what 'spots' are in range to be considered in the same track. Ultimately, the configuration of Trackmate has allowed consistent threading of 'spots' and reports all tracks and corresponding data to an Excel spreadsheet.

8.6.8. Threading Fluorescent Myosin Spots using Trackmate

Threading is the process in which we determine identity and position of an individual spot over several connected frames. Questions being asked are whether or not between these frames has this spot moved and if it has moved; has it joined to another local spot or split into two or more spots? These questions can allow us to track and follow the movement of each spot frame by frame and the decision-making behind this is mostly automated by Trackmate. However, we can adjust parameters and filters to increase the accuracy of the threading. Previously, threading each myosin was done manually and a different analysis approach was taken as mentioned in section 8.6.1. Tracking individual spots movement at a high resolution and over hundreds of frames required us to take a different approach in how we can utilise Trackmate and to validate our approach we have ran control simulations described in section 8.6.10.

8.6.9. Developing a Transition Matrix

In order to develop a transition matrix, another spreadsheet is used for analysing results gained from Trackmate. The second spreadsheet takes the results exported from Trackmate (.csv file format) and applies them to an 'Amplitude Assigning and Classification' sheet, which assigns the number of myosins based on the total intensity exhibited from each myosin spot. This is done by the lookup table made in the previous spreadsheet. Once the number of myosins are assigned, each track is grouped together by using a FILTER formula to show a track up to 50 frames in length (this can be increased if necessary). The difference between each frame is calculated using the SUM function and this information is used to classify between each frame, what is going on within an active region.

To do this, we have determined that in these conditions there are four states of myosins interaction with thin filament. Firstly, there is activation of the thin filament, this is where

one or more myosins are binding to thin filament creating an active region. Secondly, there is stepwise detachment of myosin off of thin filament, this means 1-2 myosins are leaving the active region of thin filament between each frame. Thirdly, there is a concerted release of myosin off of thin filament, this is where 2 or more myosins leave the active region between each frame. Finally, there is a chance that there is no change in the number of myosins present between each frame so we can classify that as just staying the same.

So, with these criteria set, simple IF statements are used to classify the meaning of the differences between each frame and by doing this, we can see where catastrophic collapse is taking place. Whilst doing so, we can remove results where there is no difference of myosins between each frame because when applying these results to a transition matrix, we are looking at solely the transitions between each addition or removal of myosin(s) and therefore the probability of no changes is not looked into for our studies. Another consideration we had to make was that Trackmate tracks each track until there is no local myosins to thread together anymore, therefore, the active region has ended. However, when looking at the results the data shows a normal active region and does not show the complete end of the active region. To accommodate for that, the ending of each track has been supplemented with a zero to show that from the final spot of myosin to the end the active region has collapsed completely.

With all these considerations being made, we have results which we can apply to our transition matrix on the next sheet. This sheet takes the final results from each track and by using COUNTIF functions, we are able to quantify the number of myosins transitioning between each frame. By doing so, we can work out the probability of how likely it is for a specific cluster to start at and where it would end at.

8.6.10. Analysis Suite Validation

The movement of myosin along RTF's is a very spontaneous process, in order to determine if our method of analysis works both accurately and effectively, controls were done to simulate what could potentially happen in our metastable conditions. A track is defined as a single spot along several frames that has been followed and threaded by Trackmate. A myosin molecule can join another track, split into two or more tracks, multiple tracks can move in parallel simultaneously, and all conditions can have a random level of unbiased bidirectional displacement (Desai *et al.*, 2015) between each frame.

Here I will outline 3 scenarios that we can anticipate seeing in actual data. A single track can remain static over a period of frames. A single track can split, hence generating two or more tracks or the opposite can occur where two tracks spatially close enough can join together and merge into a single track. Whilst bidirectional displacement of myosin molecules occurs, this is accommodated for in section 8.6.7

We have generated control scenarios that are 20 frames each – in turn giving us enough frames to provide splitting or merging two tracks for example. The aim of these control scenarios is to validate the accuracy of our analysis approach by comparing the positional

and intensity values we have inputted versus what has ultimately been tracked and threaded by Trackmate. This is illustrated in section 9.2.1.

In every case, our method of analysis gave us 1:1 tracking when using Trackmate. By calculating the difference between the inputted data versus the data we gained from tracking, the closer the value is to 0, the closer the tracked positional value is to the inputted value. In all cases these differences were 0 and the corresponding intensity values were also correct.

9. Results

9.1. Extraction and Purification Analysis:

9.1.1. Extraction of myosin from chicken pectoralis

Myosin was extracted from chicken pectoralis; the process took 3 days starting off with 335.8 g of tissue and ending with 12.2 g (~ 12 ml) of 19.3 µM myosin, providing a percentage yield of 3.6%. A time course of the extraction process was done where samples were taken across the process and an SDS-PAGE gel was done at the end (see figure 8). In Figure 8, our lane of interest is Stage 10, which is the final step in the clarification of myosin, there are several bands present labelled 1-5 which consists of myosin's heavy chains, tropomyosin, actin, ELC, and RLC, respectively. Considering this gel has overloaded samples, we can see faint bands of actin and tropomyosin, but we can consider the concentration of these to be low enough to not cause any concern.

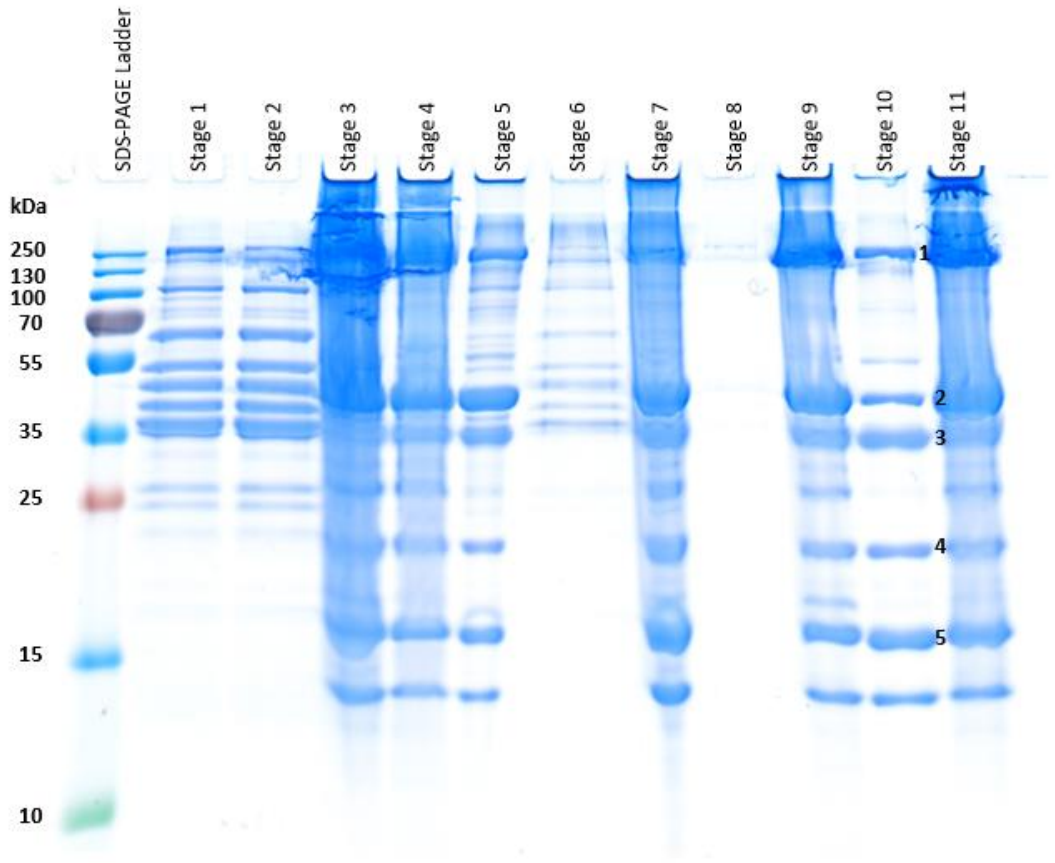

Figure 8 - 15% SDS-PAGE gel showing a chronological compendium of processes to extract myosin from chicken pectoralis.

Banding patterns are related to actomyosin products, throughout the extraction process – each stage is further described in section 8.1.1. Although this gel was overloaded, it still highlights the bands of interest in Stage 10. Stage 10 shows 5 bands of interest, where 1 is the heavy chain of myosin (220 kDa), band 2 is actin (42 kDa), band 3 is tropomyosin (65 kDa), band 4 is the essential light chain (22.8 kDa), and band 5 is the regulatory light chain (18.8 kDa).

weight of myosin was determined from literature to be 493,000 Da (Holtzer and Lowey, 1959).

Table 2 - Spectrophotometry values to determine the concentration of myosin.

Serial dilutions were made, allowing three sets of values to be averaged. The absorbances were measures at 280 nm and 320 nm to then calculate the concentration of myosin in mg/ml and as a molarity.

Dilution	Abs_{280}	Abs_{320}	mg/ml	µM
1:25	0.341	0.93	8.3	16
1:50	0.191	0.051	9.5	19
1:100	0.107	0.026	11.4	23
Average	-	-	**9.7**	**19.3**

9.1.2. Papain digest of full-length myosin into S1-myosin

Extracted myosin must be digested into S1-myosin to be used in subsequent exchange reactions that fluorescently label it for our studies. Papain is the proteolytic enzyme that has proven to be consistent and useful for cleavage of full-length myosin into S1-myosin. Figure 9 shows a time course of the digestion and although this gel has been overloaded and HMM can be seen labelled band 1, however its intensity in comparison to the start of the process has dramatically decreased suggesting the concentration of it is negligible.

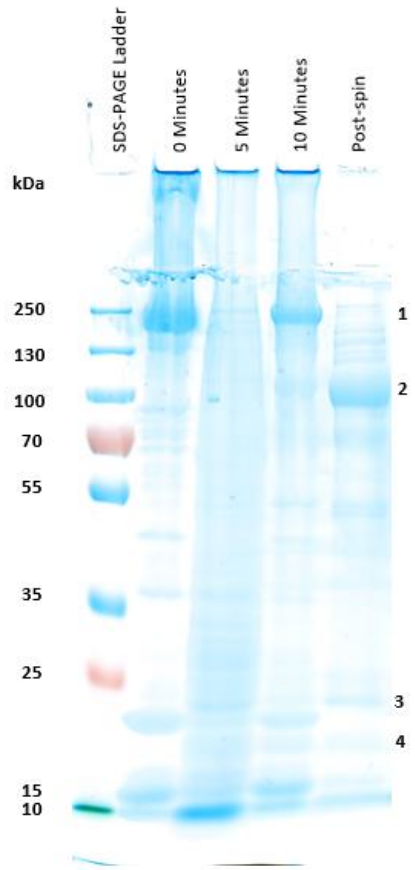

Figure 9 - 10% SDS-PAGE gel showing the time-course of myosin digestion using papain.

This is where we took samples every 5-minutes, a different composition of components can be seen over time. In our final sample, we spun down the S1 after an overnight dialysis step in preparation for further column purification. In the final 'Post spin' well, we can see four main bands of interest. Again, this gel has been overloaded but we can see band 1 being some remnants of heavy chain myosin (220 kDa), band 2 is S1-myosin (97 kDa), band 3 being ELC (22. 8 kDa) and 4 being RLC (18.8 kDa).

9.1.3. Purification of actin from acetone powder

Acetone powder is derived from the pulp saved from the myosin preparation. It was processed via a series of steps into actin which is seen in 'Stage 7'. The arrow indicates actin which is about 42 kDa in size.

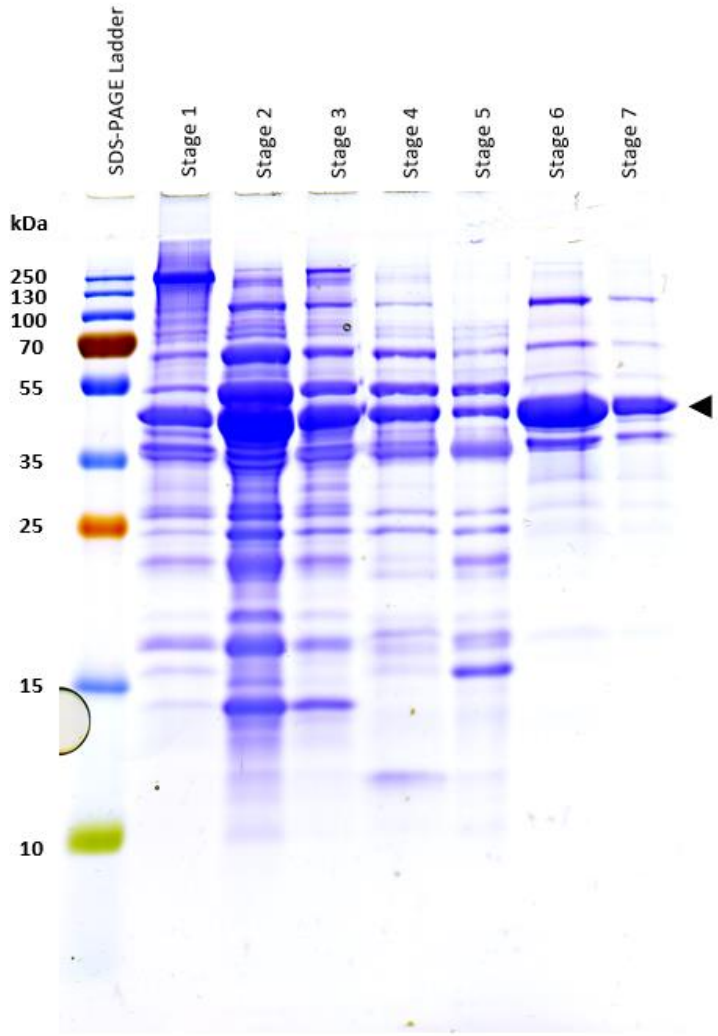

Figure 10 - Time-course of actin preparation from acetone powder.

This shows the different stages when preparing actin from acetone powder, resulting in the final well (Stage 7) being relatively pure despite overloading of wells. The arrow indicates actin with the molecular weight of 42 kDa.

9.1.4. Creating the RLC-mNeonGreen-6xHis plasmid

We were successfully able to create this RLC-mNeonGreen-6xHis plasmid by using two constructs, one being a plasmid with RLC attached to mScarlet (see Figure 11), the other being a plasmid with a protein called UvrB attached to mNeonGreen (see Figure 12). The aim was to use Polymerase Chain Reaction (PCR) to eliminate the mScarlet in the first plasmid and in the other plasmid the plan was to conserve only mNeonGreen whilst adding extensions that are complementary to the RLC plasmid. By doing this, we have created a vector and an insert, which are the RLC plasmid and extended mNeonGreen, respectively. Now, we can use a Gibson Assembly process to connect the two together, use colony PCR to detect the size of our new plasmid, to then miniprep and sequence our RLC-mNeonGreen-6xHis plasmid. Each step is outlined below.

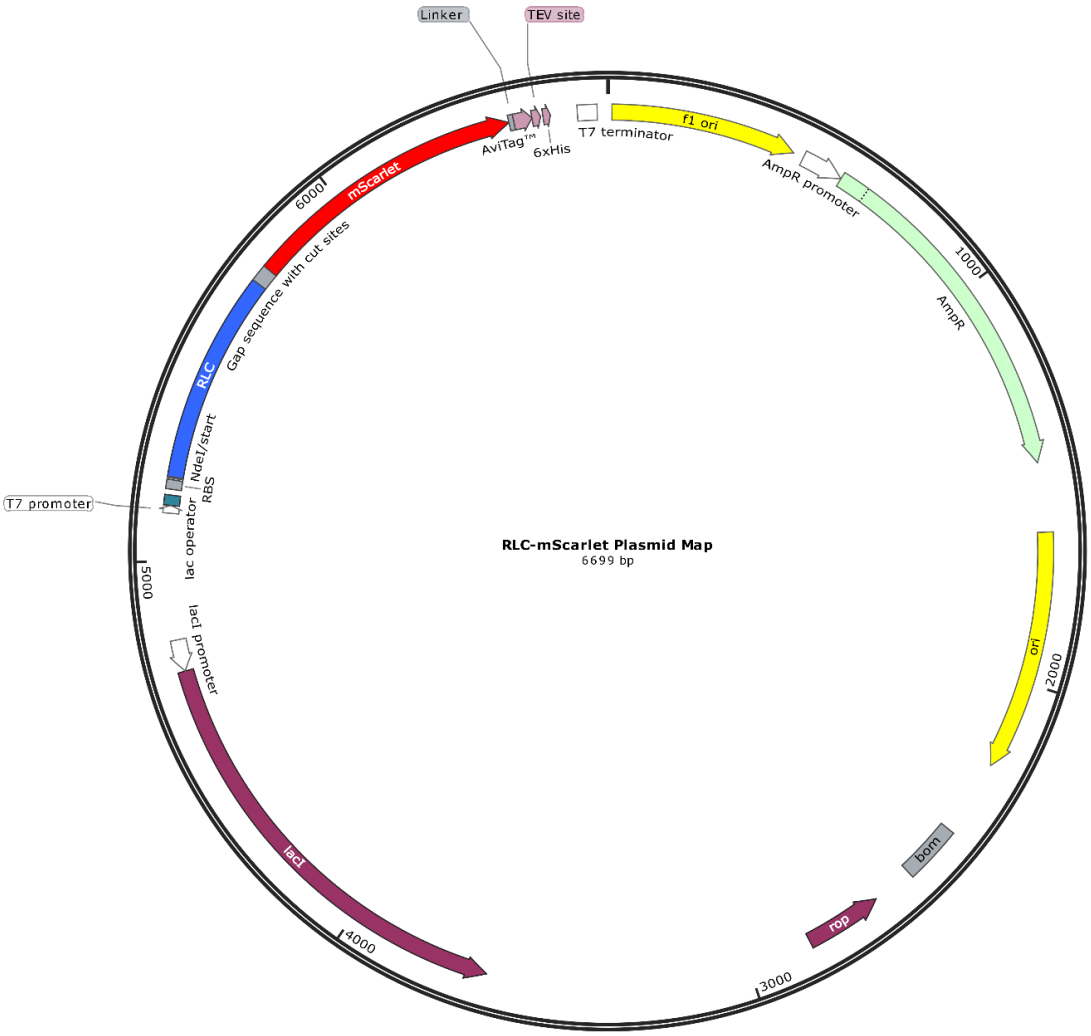

Figure 11 - RLC-mScarlet plasmid map.

This illustrates the vector that we are starting with before linearisation, the aim is to remove the mScarlet portion (coloured red).

This is the RLC-mScarlet plasmid, which will act as our vector for our final product. The aim is to remove the mScarlet via PCR whilst retaining all other features including the GAP sequence prior to the mScarlet and the AviTag, 6xHis and TEV site after it. Also, it has the ampicillin resistance gene so we can selectively choose for it when conducting expression and purification of the protein.

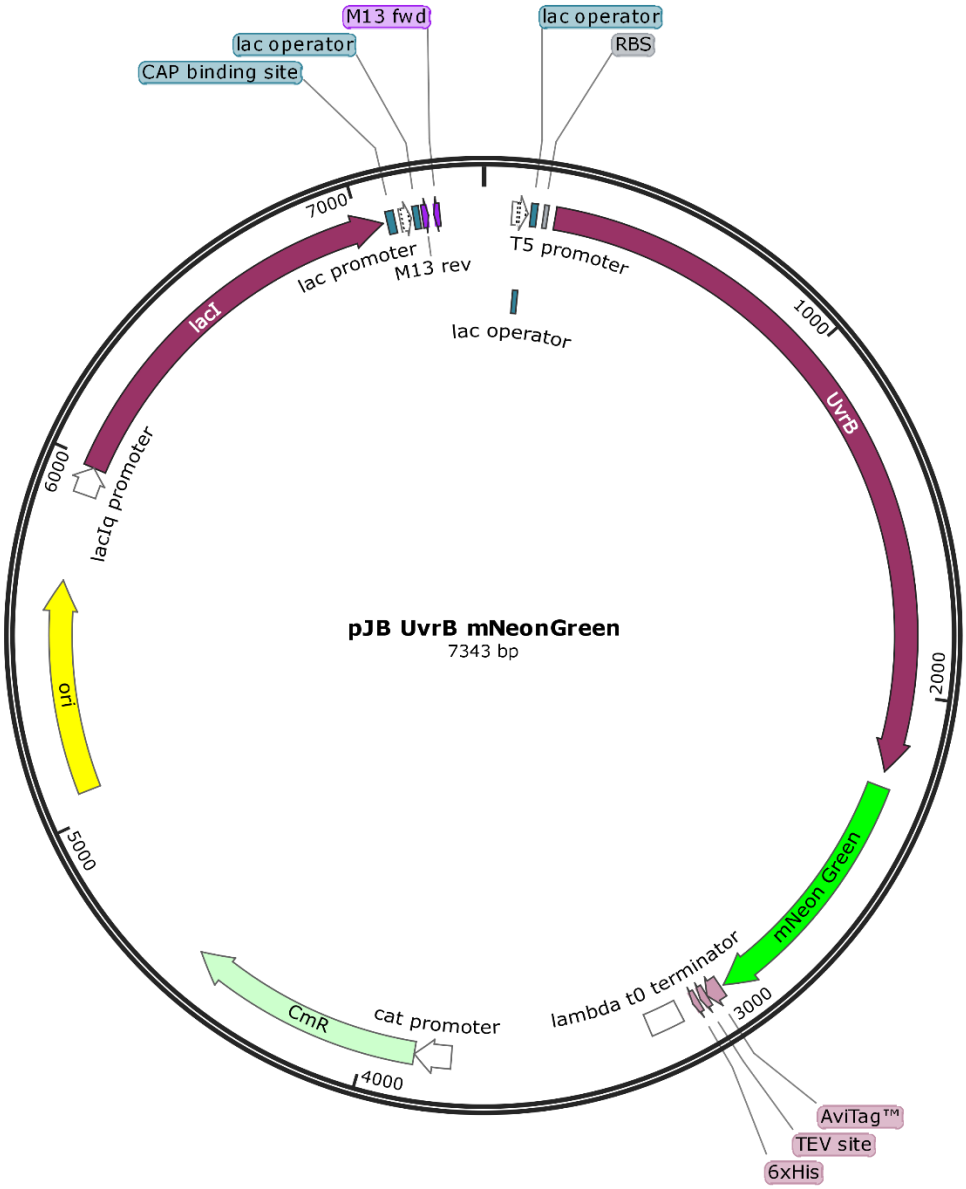

Figure 12 – This is the UvrB-mNeonGreen plasmid map.

The aim for this plasmid would be to isolate the mNeonGreen portion with primers that extend to create a complementary overhang to the linear vector we made previously.

This is the UvrB-mNeonGreen plasmid, which contains the mNeonGreen which we want to isolate, using PCR we are able to do so, and we are able to create extensions on the mNeonGreen portion allowing complementarity to our RLC plasmid vector.

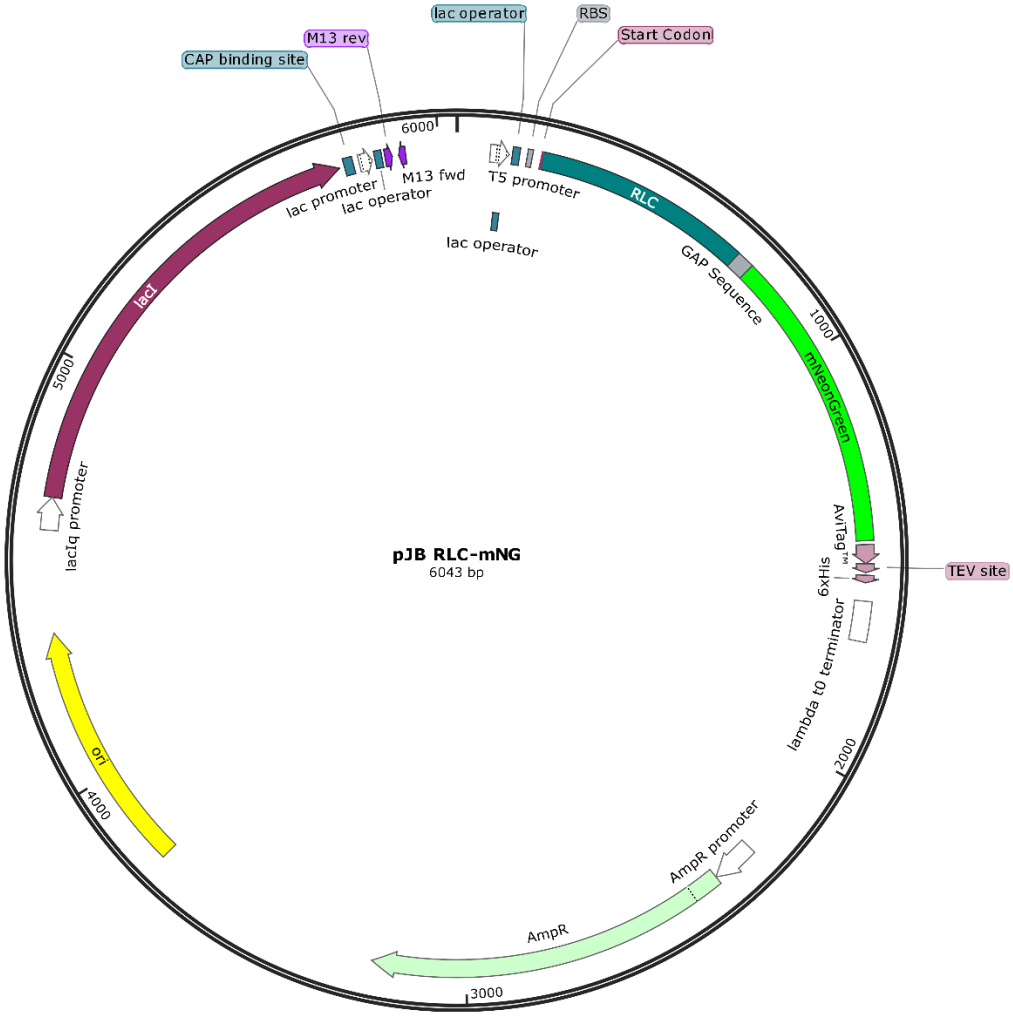

Figure 13 - This is the desired plasmid, RLC-mNeonGreen.

After several PCR reactions and Gibson Assembly, we aim to have this as a plasmid. This has been confirmed via sequencing.

Figure 13 shows the desired plasmid we aim to create from dissecting and combining the two plasmids mentioned earlier. This plasmid has successfully been made via Gibson Assembly, sequenced by Eurofins Genomics and sequences were verified manually using Snapgene.

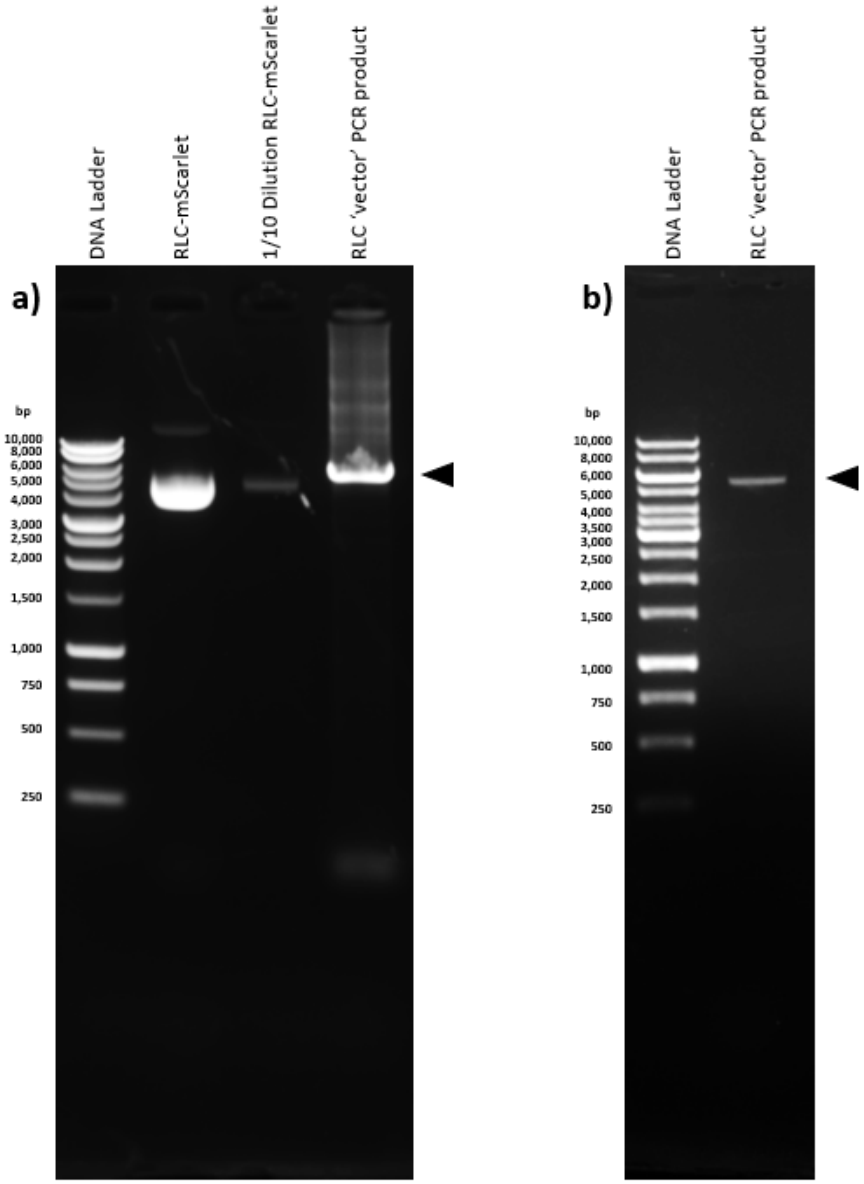

Figure 14 - Using PCR to remove mScarlet from RLC-mScarlet.

a) Highlights the initial PCR reaction, the final well shows our desired band, but there seems to be smearing at the higher molecular weights are present as well as primer dimers at the end of the gel. However, in b) this is cleared up by using a QIAgen DNA extraction and purification kit to solely isolate our desired PCR product.

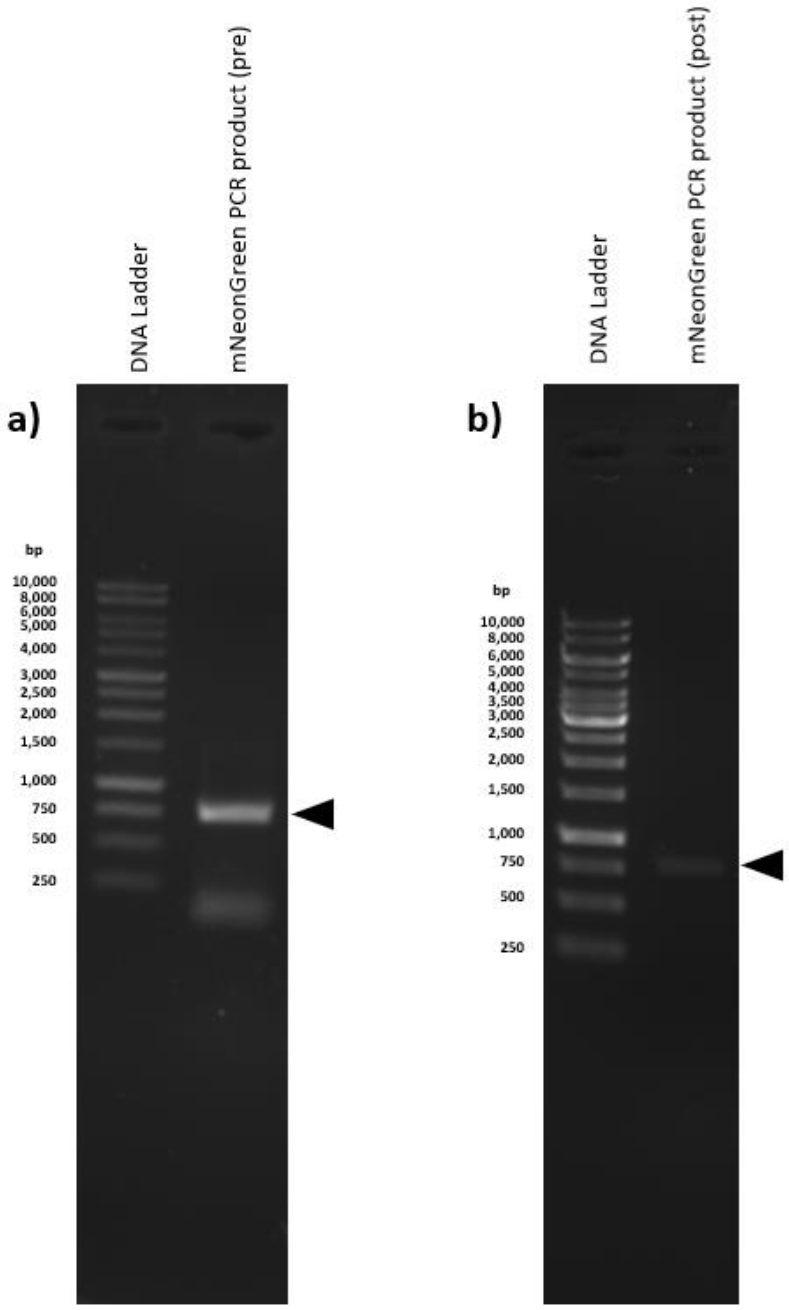

Figure 15 - PCR of UvrB-mNeonGreen to isolate mNeonGreen and create complementary overhangs to the linearised vector.

a) Shows the initial PCR reaction, with our desired PCR product highlighted with the arrow, however, primer dimers are seen below so it was decided a PCR clean-up was necessary. b) Shows the clean isolate of mNeonGreen with complementary overhangs.

Standard PCR reactions were done for both Figures 14 and 15, in both cases we do see primer dimers and a varying degree of 'smearing', however, this is not an issue due to Gel Extraction PCR purification kits provided by QIAgen. The desired band can be cut out using a transilluminator and purified as seen in part b) of each Figure 14 and 15. Their concentrations have been quantified via spectrophotometry and are the following: Vector – 10 ng/µl and Insert – 25 ng/µl.

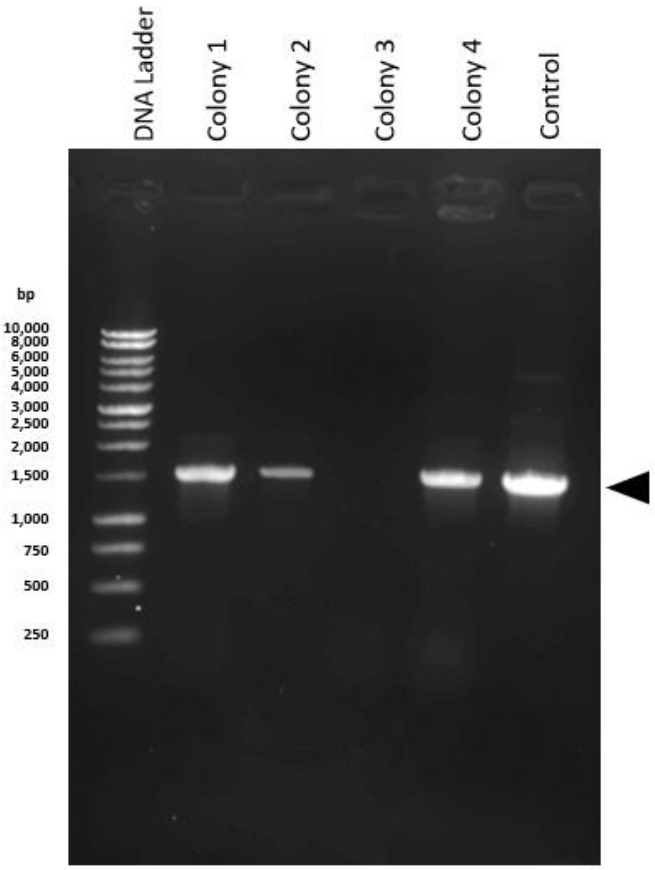

Figure 16 - Colony PCR of RLC-mNeonGreen after Gibson Assembly.

Three out of four colonies have our desired plasmid, showing a consistent banding pattern and it follows a similar size as the control which is RLC-mScarlet. The bands of interest are highlighted by the arrow. Colonies 1 and 4 were chosen to miniprep as colony 2 was fainter than the rest and colony 3 did not contain our plasmid of interest.

Colony PCR is a convenient procedure to determine whether a Gibson Assembly has been successful after transformation. Using primers that can seek out our RLC-mNeonGreen enables us to see it amplified on our agarose gels. In addition to visualising it on a gel, each colony has been streaked onto an agar plate with complementary antibiotic resistance and the streak patterns did verify what was seen in the agarose gel in Figure 16.

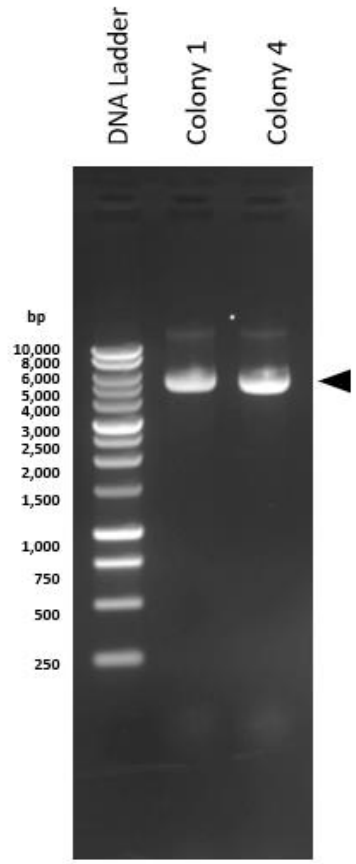

Figure 17 - Miniprep of Colonies 1 and 4.

Successful minipreps can be seen where the arrow highlights the band of interest being our RLC-mNeonGreen.

Considering our colony PCR was successful, the colony was grown in LB broth and plated to ultimately be miniprepped using a QIAgen Miniprep Kit. Using a Expedion Versawave 2 spectrophotometer, we are able to quantify our miniprepped plasmid. We achieved 70 ng/µl concentrated plasmid which seems plausible due to the intensity of the bands in Figure 17. After the successful miniprep, we sent a sample off to be sequenced by Eurofins Genomics and results were received and sequences were verified manually using Snapgene.

9.1.5. Expression of RLC-mNeonGreen-6xHis

Typical expression of a protein would not yield a significant amount of our desired protein of interest from our plasmid. Therefore, we use a compound called Isopropyl β-d-1-thiogalactopyranoside (IPTG) which essentially mimics allolactose from the *lac* operon and induces high levels of protein expression. This in turn allows a significant increase of our protein of interest as seen in Figure 18.

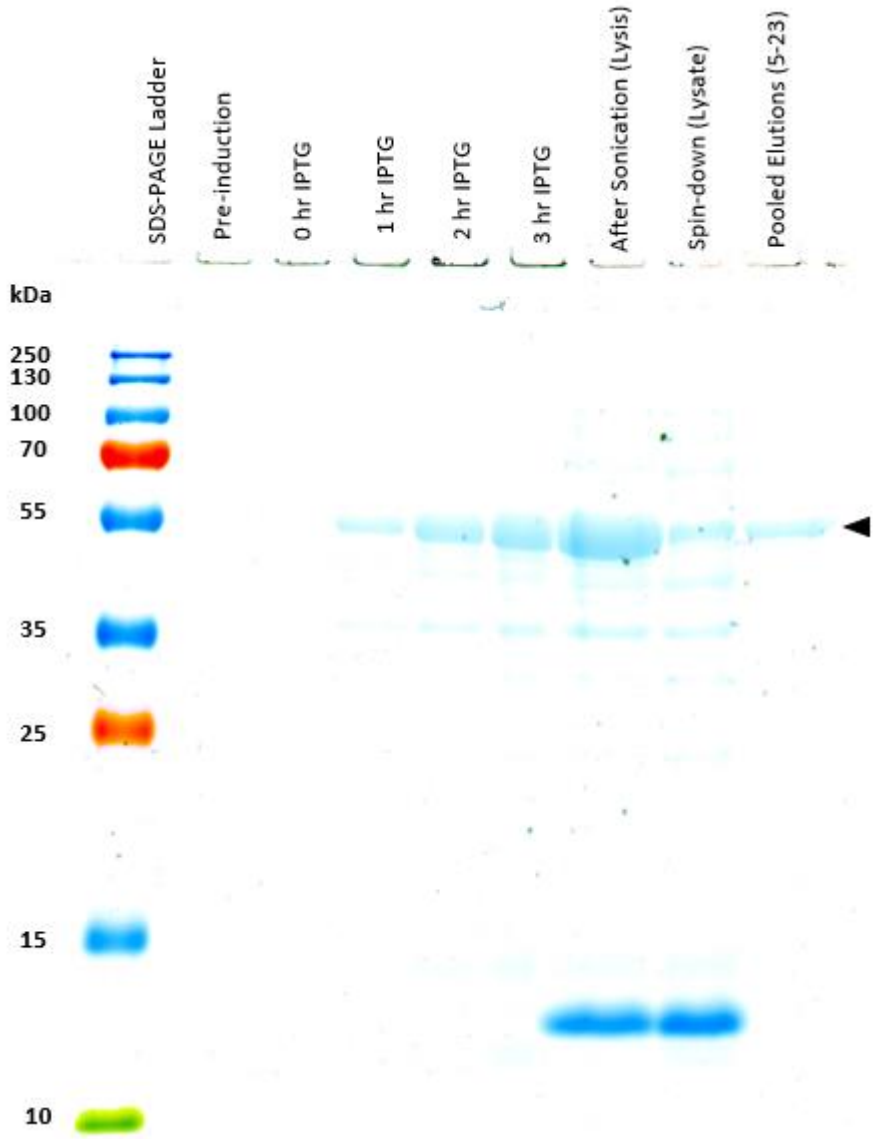

Figure 18 - Time-course 12.5% SDS-PAGE gel of expression and induction of RLC-mNeonGreen using IPTG.

A three-hour induction with IPTG was done to induce protein expression, our protein of interest was expressed as highlighted by the arrow. Subsequent wells are labelled accordingly and are in reference to purification of RLC-mNeonGreen. The intense band appearing from sonication and spinning down the cells suggests something from the cellular debris has accumulated.

9.1.6. Purification of RLC-mNeonGreen-6xHis

The final step revolves around purifying our expressed RLC-mNeonGreen-6xHis, this is done by immobilised metal affinity chromatography (IMAC). Where a prepacked HisTrap column (GE Healthcare) allows immobilised Nickel to bind and release our His-tagged protein over an elution gradient.

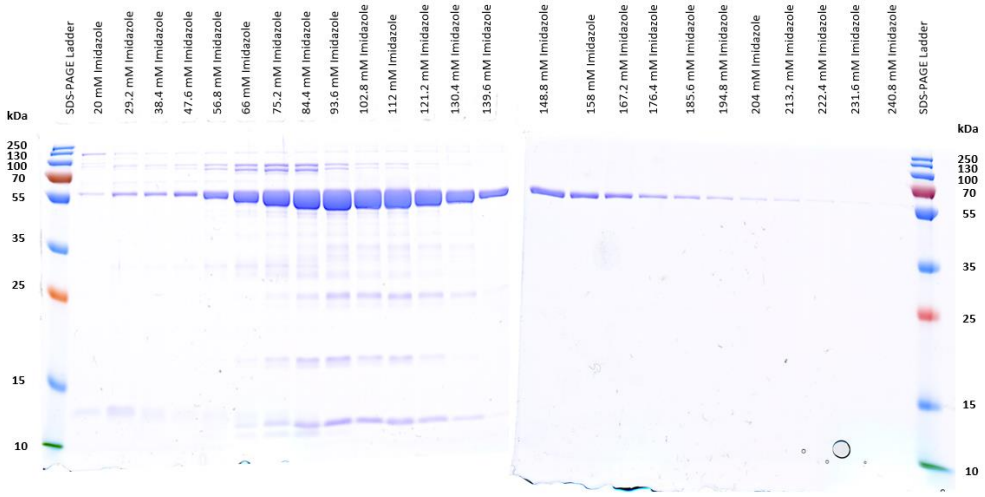

Figure 19 - 12.5% SDS-PAGE gel showing an elution profile for purification of RLC-mNeonGreen-6xHis.

Using a GE Healthcare HisTrap HP protein purification column allowed separation of our RLC-mNeonGreen-6xHis protein over an elution gradient. Fractions 5-23 were pooled, and spectrophotometry was done to determine its final concentration of 1.62 µM.

9.2. Data Analysis:

9.2.1. Validating the analysis methodology

In order to determine if our method of analysis is accurate, we conducted three sets of controls, as describe in section 8.6.10. The controls were upscaled from 30 px width to 300 px, and Trackmate successfully tracked and threaded each track with correct intensity and positional values. For illustrative purposes, an example of a kymograph has been shown in

Figure 21, where there are there are plenty of individual spots that are super-resolved by our analysis process to be tracked using Trackmate.

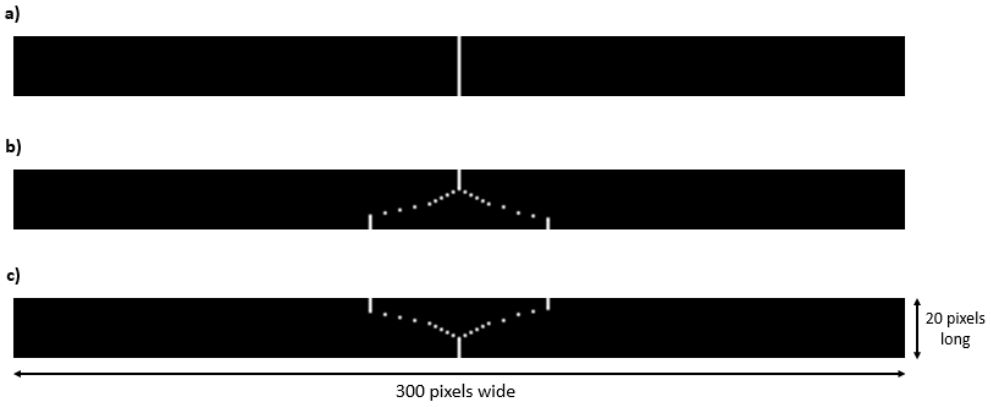

Figure 20 - Simulated kymographs to act as controls to determine the accuracy of Trackmate tracking and threading.

Where a) is a track of simulated fluorescent myosin as a static straight line, b) is simulated myosin departing and splitting into two tracks and c) is the opposite where initially two tracks join together and merge into a single track. The kymographs have been upscaled by a factor of 10 to consider sub-pixels, where the original scale was 30 px wide by 20 px length, it is now 300 px wide and 20 px length.

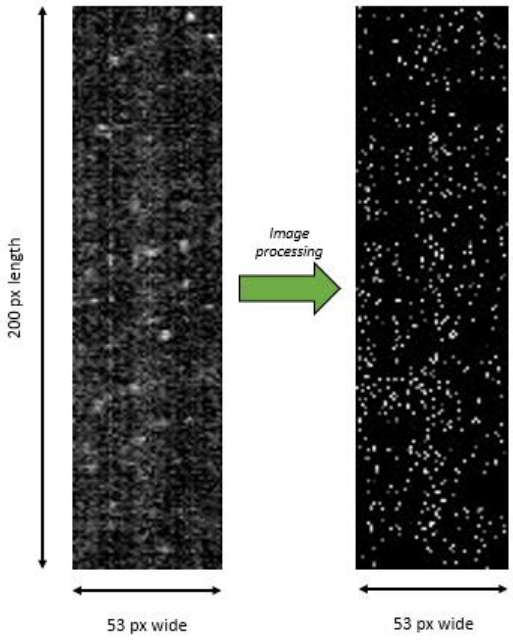

Figure 21 - Example before and after kymographs illustrating the kymographic data in full that would be tracked using Trackmate.

Kymographic data has been processed by our method of analysis (left to right), prior to using Trackmate this is something that would be sliced into their respective frames and converted into a .mj2 movie. For illustrative purposes, this kymograph is not scaled up by a factor of 10. The left kymograph shows the kymographic data in result from initial conversion of imaged data to kymographic projections. On the right is after image processing and analysis, an illustration of what the data would look like if not scaled up as mentioned previously.

9.2.2. Thin filament supplemented with tropomyosin

To investigate the propensity of catastrophic collapse, videos were analysed from a range of S1 myosin concentrations (5-20 nM), at metastable conditions of 5 nM S1, clusters were extremely sparse and imaging conditions were subject to high background noise, making it difficult for our analysis suite to pick out individual myosin clusters. To overcome this, we found a 'sweet-spot' of 15 nM S1 to clearly visualise and determine the transitioning of cluster sizes.

Final Cluster Size - Tropomyosin (only) Thin Filament

Start Cluster Size	0	1	2	3	4	5	6
1	0.38	0.00	0.34	0.12	0.10	0.04	0.03
2	0.30	0.36	0.00	0.15	0.11	0.04	0.04
3	0.25	0.26	0.31	0.00	0.13	0.02	0.03
4	0.26	0.26	0.25	0.15	0.00	0.04	0.03
5	0.27	0.31	0.26	0.08	0.05	0.00	0.02
6	0.25	0.32	0.26	0.06	0.05	0.05	0.00

Legend
0.00
0.08
0.15
0.23
0.30
0.38

Figure 22 - Measured transitions between cluster sizes of tropomyosin supplemented RTFs.

Our new method of analysis allows us to get this set of data. Whereby, this transition matrix shows us the probability of starting at 1 myosin and ending at a maximum cluster size of 6 myosins. The central diagonal zero shows that the probability of a molecule staying the same size is not considered because it is not a transition between cluster sizes. The starting cluster size of zero is omitted because we are unable to determine when a track starts. Final cluster sizes show that accelerated release of myosin is mediated mostly by tropomyosin. Data obtained here was at 15 nM S1-GFP at 0.1 µM ATP (N = 10).

9.2.3. Thin filament supplemented with tropomyosin and troponin

To investigate the propensity of catastrophic collapse, videos were analysed at metastable conditions of 5 nM S1, 0.1 µM ATP and pCa 6. In comparison to Fig 22, catastrophic collapse seems to have an elevated final cluster size of two myosins suggesting an intermediate state (an energy trap) to catastrophic collapse mediated by the presence of troponin. However, further investigations using super-resolution techniques would be required to delve deeper to this initial observation.

Final Cluster Size - Regulated Thin Filament

Start Cluster Size	0	1	2	3	4	5	6
1	0.26	0.00	0.56	0.10	0.07	0.01	0.00
2	0.37	0.33	0.00	0.17	0.09	0.02	0.01
3	0.21	0.18	0.52	0.00	0.07	0.01	0.01
4	0.16	0.19	0.43	0.17	0.00	0.05	0.01
5	0.17	0.15	0.41	0.11	0.15	0.00	0.01
6	0.18	0.11	0.38	0.15	0.13	0.05	0.00

Legend
0.00
0.11
0.22
0.33
0.45
0.56

Figure 23 - Measured transitions between cluster sizes for tropomyosin and troponin supplemented RTFs.

Our new method of analysis allows us to get this set of data. Whereby, this transition matrix shows us the probability of starting at 1 myosin and ending as maximum of 6 myosins. The central diagonal zero shows that the probability of a molecule staying the same size is not considered because it is not a transition between cluster sizes. The starting cluster size of zero is omitted because we are unable to determine when a track starts. Data obtained here was at 5 nM S1-GFP at 0.1 µM ATP (N = 14).

9.2.4. Catastrophic collapse at varying cluster sizes

Catastrophic collapse has been measured by using the values from the first column of the transition matrices from Figures 22, 23 and from previous studies.

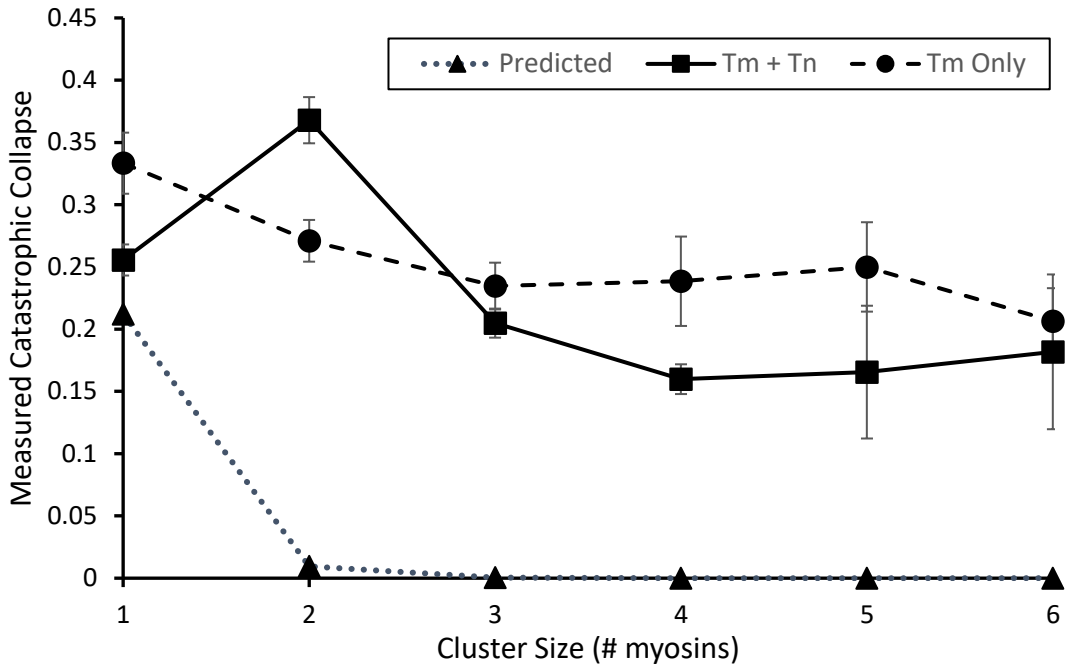

Figure 24 – A graph illustrating the probability of predicted and measured catastrophic collapse of RTFs.

The first column from Figures 22 and 23 are used to illustrate black dashed line with circle points and the solid black line with square points respectively, previous studies results (Inchingolo *et al.*, 2018) are shown in the blue dotted line with triangle points.. Essentially, we can see that on average thin filament supplemented with tropomyosin only is sufficient for the concerted release of myosin as we see higher probabilities of measured catastrophic collapse.

10. Discussion

The activation and deactivation of thin filament has been studied extensively over the years (Geeves and Lehrer, 1994; Maytum *et al.*, 1999; Desai *et al.*, 2015; Inchingolo *et al.*, 2018; Inchingolo *et al.*, 2019), advances in structural studies (Galińska-Rakoczy *et al.*, 2008; Ratti *et al.*, 2011; Yang *et al.*, 2014; Von Der Ecken *et al.*, 2015) provide ideas on the regulatory aspect of muscular contraction. Whilst heart diseases such as HCM are still prevalent, it provides an urgency to understand the fundamental mechanism of muscular contraction. Our studies aim to provide a mechanistic insight on this whilst investigating a newly discovered phenomenon termed catastrophic collapse. Regulated thin filament in our *in vitro* system provides us the ability to visualise the cooperative activation, stepwise deactivation, and catastrophic collapse of an active myosin cluster. RTFs consists of the regulatory components tropomyosin and troponin which can sense calcium to control the activation and deactivation of thin filament. Our method of analysis allows us to observe these clusters fluctuating in size and in some cases collapsing entirely. After a closer inspection of our results using transition matrices, we see that there is a higher proportion of concerted myosin release suggesting that there is another method of deactivation other

than traditional stepwise deactivation. This was suggested in previous studies using the RJMCMC approach (Inchingolo *et al.*, 2018), and our method of analysis not only confirms the previous results but enhances it by looking at not only RTFs with troponin and tropomyosin but thin filament with just tropomyosin. The reasoning behind looking at both can show us the importance of these regulatory factors during catastrophic collapse and can allow us to get a better understanding of heart diseases such as hypertrophic cardiomyopathy (HCM).

Our well-rounded approach to this study involves looking at myosin interactions on all the possible thin filament compositions; free thin filament (without tropomyosin and troponin), thin filament supplemented with tropomyosin and thin filament with both tropomyosin and troponin. However, without the regulatory proteins to control myosin binding in free actin, it would not provide the metastable environment needed to investigate the cooperative activity of myosin. In previous studies, it has been shown that, free actin even in the presence of a low myosin concentration (1 nM) has extremely frequent myosin binding (Desai *et al.*, 2015). Therefore, we can deduce that free actin is not a state in which provides these conditions to allow us to investigate our hypotheses. This further supports our hypotheses that the concerted release of myosin revolves around the presence of the regulatory proteins tropomyosin and troponin.

Tropomyosin accelerates catastrophic collapse:

Tropomyosin is considered as a rigid gatekeeper (Sousa *et al.*, 2010) meaning it has an effect on thin filament activation. Studies have considered tropomyosin to be a semi-rigid molecule by conducting various measurements of its persistence length (Swenson and Stellwagen, 1989; Phillips and Chacko, 1996; Li *et al.*, 2010b; Sousa *et al.*, 2010), its rigidity has been considered enough to act as a cooperative unit allowing shifting between regulatory states (Li *et al.*, 2010a). Thin filament supplemented with tropomyosin only, lacks the troponin complex to calcium sense and regulate conformational change along thin filament. Therefore, we can hypothesise that tropomyosin alone on thin filament is capable of accelerating catastrophic collapse, shifting itself into the blocked state of the three-state model. Recent studies illustrate this using molecular dynamics and cryo-EM (Kiani *et al.*, 2019)and our analysis support this and shows that tropomyosin alone has a high chance to orchestrate catastrophic collapse (Figure 24). Beneath the zeroed diagonal in the transition matrix, shows a high probability of finishing at a lower cluster size than what the cluster size started at, this is highlighted by the varying degrees of red in Figure 22. This suggests there is a higher probability of myosin molecules being shifted off an active region. This supports our hypothesis, because we can see that tropomyosin alone can cause thin filament to shift towards the blocked state causing catastrophic collapse. Tropomyosin is able to oscillate laterally over thin filament (McKillop and Geeves, 1993), it is believed that structural studies have underestimated the stiffness of tropomyosin due to their measurements of the persistence length as a straight rod instead of its superhelical conformation (Lehman *et al.*, 2020). Therefore, we can suggest that now more realistic considerations of tropomyosin's curved superhelical persistence length of 423 nm leads to reasoning that tropomyosin is stiffer and causes an increased likelihood of being in a B-state position. Where the B-state position (Lehman *et al.*, 2009) of tropomyosin is comparably the blocked state of the three-state model of thin filament activation.

The troponin complex has a tighter regulation on catastrophic collapse:

Thin filament was also supplemented with both tropomyosin and troponin; this provides us all the necessary components for thin filament activation. Whereby RTFs are in equilibrium between closed and open state due to the local presence of ATP, calcium and myosin. Figure 24 shows that there is a decrease in catastrophic collapse upon the addition of troponin, this suggests that troponin can sense calcium in our metastable conditions, allowing tropomyosin to be more inclined to move between the closed and open states. On a mechanistic level, we can suggest that the presence of activated troponin allows tropomyosin to stay in an open conformation allowing myosin to bind and release as normal. However, as the thin filament moves into the closed state, there is a chance that troponin may deactivate causing tropomyosin to release all remaining myosin attached onto thin filament. Structural studies have determined that the tip of the TnI domain interacts with tropomyosin and stabilises the blocked state configuration (Galińska-Rakoczy *et al.*, 2008), which allows us to suggest that if we are in the closed state and troponin C deactivates, TnI will stabilise the blocked state configuration thus enabling catastrophic collapse. We can suggest that the troponin complex acts as a regulator for catastrophic collapse because of the balancing that is done between all three subunits of troponin. Whilst TnC has an increased affinity for Ca^{2+} ions (Galińska-Rakoczy *et al.*, 2008), TnT structurally strengthens tropomyosin to act as a cooperative unit (Sousa *et al.*, 2010), and TnI in the closed state enables the shift of tropomyosin into the blocked state (Galińska-Rakoczy *et al.*, 2008). We have shown that the addition of the troponin complex decreases the probability of catastrophic collapse occurring but does not completely abolish it. The fact that catastrophic collapse can occur suggests that it is a necessary process to maintain the homeostasis of muscular contraction.

11. Conclusion

Our study combines single molecule microscopy and a powerful analysis suite to investigate the concerted release of myosin on regulated thin filament. Developing a new method of analysis enables us to provide a high throughput and simpler approach to processing our imaging data. The new method of analysis has illustrated the prevalence of catastrophic collapse in regulated thin filaments. Following the previous studies using the RJMCMC approach (Inchingolo *et al.*, 2018), our data falls in line with what was previously stated and develops it by looking into individual components of regulation such as tropomyosin. The surprising finding from our results is that thin filament only supplemented with tropomyosin seem to have a higher probability of catastrophic collapse. This study can act as an insight on diseases such as hypertrophic cardiomyopathy (HCM) which has been seen to be caused by molecular insults with tropomyosin. The E180G mutation on tropomyosin causes a reduced rigidity of tropomyosin (Li *et al.*, 2012) which causes an impairment of muscular relaxation. Catastrophic collapse can be considered as an essential process to ensure muscular relaxation is not compromised and this phenomenon can provide a mechanistic insight to HCM.

12. References:

Au, Y. (2004) The muscle ultrastructure: a structural perspective of the sarcomere. *C Cell Mol Life Sci* **61**: 3016–3033.

Bailey, K. (1946) Tropomyosin: A new asymmetric protein component of muscle [2]. *Nature* **157**: 368–369 https://www.nature.com/articles/157368b0.

Barua, B., Winkelmann, D. a., White, H.D., and Hitchcock-DeGregori, S.E. (2012) Regulation of actin-myosin interaction by conserved periodic sites of tropomyosin. *Proc Natl Acad Sci* **109**: 18425–18430.

Berchtold, M.W., Brinkmeier, H., and Müntener, M. (2000) Calcium ion in skeletal muscle: Its crucial role for muscle function, plasticity, and disease. *Physiol Rev* **80**: 1215–1265 www.physrev.physiology.org.

Bezprozvanny, I., Watras, J., and Ehrlich, B.E. (1991) Bell-shaped calcium-response curves of Ins(l,4,5)P3- and calcium-gated channels from endoplasmic reticulum of cerebellum. *Nature* **351**: 751–754 https://pubmed.ncbi.nlm.nih.gov/1648178/.

Biesiadecki, B.J., Davis, J.P., Ziolo, M.T., and Janssen, P.M.L. (2014) Tri-modal regulation of cardiac muscle relaxation; intracellular calcium decline, thin filament deactivation, and cross-bridge cycling kinetics. *Biophys Rev* **6**: 273–289.

Bootman, M.D. (2012) Calcium signaling. *Cold Spring Harb Perspect Biol* **4**: 1–3 /pmc/articles/PMC3385957/?report=abstract.

Brown, J.H., Zhou, Z., Reshetnikova, L., Robinson, H., Yammani, R.D., Tobacman, L.S., and Cohen, C. (2005) Structure of the mid-region of tropomyosin: Bending and binding sites for actin. *Proc Natl Acad Sci U S A* **102**: 18878–18883 www.pnas.orgcgidoi10.1073pnas.0509269102.

Dasgupta, A., and Wahed, A. (2014) Cardiac Markers. In *Clinical Chemistry, Immunology and Laboratory Quality Control*. Elsevier, pp. 127–144.

Desai, R., Geeves, M.A., and Kad, N.M. (2015) Using fluorescent myosin to directly visualize cooperative activation of thin filaments. *J Biol Chem* **290**: 1915–1925.

Dillon, P.F., Aksoy, M.O., Driska, S.P., and Murphy, R.A. (1981) Myosin phosphorylation and the cross-bridge cycle in arterial smooth muscle. *Science (80-)* **211**: 495–497 https://pubmed.ncbi.nlm.nih.gov/6893872/.

Dominguez, R., and Holmes, K.C. (2011) Actin structure and function. *Annu Rev Biophys* **40**: 169–186 http://www.annualreviews.org.

Ecken, J. Von Der, Müller, M., Lehman, W., Manstein, D.J., Penczek, P.A., and Raunser, S. (2015) Structure of the F-actin-tropomyosin complex. *Nature* **519**: 114–117 https://www.nature.com/articles/nature14033.

Finch, E.A., Turner, T.J., and Goldin, S.M. (1991) Calcium as a coagonist of inositol 1,4,5-trisphosphate-induced calcium release. *Science (80-)* **252**: 443–446 https://pubmed.ncbi.nlm.nih.gov/2017683/.

Fusi, L., Brunello, E., Yan, Z., and Irving, M. (2016) Thick filament mechano-sensing is a calcium-independent regulatory mechanism in skeletal muscle. *Nat Commun* **7** www.nature.com/naturecommunications.

Galińska-Rakoczy, A., Engel, P., Xu, C., Jung, H.S., Craig, R., Tobacman, L.S., and Lehman, W.

(2008) Structural Basis for the Regulation of Muscle Contraction by Troponin and Tropomyosin. *J Mol Biol* **379**: 929–935 /pmc/articles/PMC2483953/?report=abstract.

Geeves, M.A. (2012) Thin filament regulation. In *Comprehensive Biophysics*. Elsevier Inc., pp. 251–267 https://linkinghub.elsevier.com/retrieve/pii/B9780123749208004161.

Geeves, M.A., Chai, M., and Lehrer, S.S. (2000) Inhibition of actin-myosin subfragment 1 ATPase activity by troponin I and IC: Relationship to the thin filament states of muscle. *Biochemistry* **39**: 9345–9350 https://pubs.acs.org/sharingguidelines.

Geeves, M.A., and Holmes, K.C. (1999) Structural mechanism of muscle contraction. *Annu Rev Biochem* **68**: 687–728 www.annualreviews.org.

Geeves, M.A., and Lehrer, S.S. (1994) Dynamics of the muscle thin filament regulatory switch: the size of the cooperative unit. *Biophys J* **67**: 273–282.

Greenberg, M.J., and Moore, J.R. (2010) The molecular basis of frictional loads in the in vitro motility assay with applications to the study of the loaded mechanochemistry of molecular motors. *Cytoskeleton* **67**: 273–285 https://www.ncbi.nlm.nih.gov/pmc/articles/PMC2861725/.

Gunning, P.W., Ghoshdastider, U., Whitaker, S., Popp, D., and Robinson, R.C. (2015a) The evolution of compositionally and functionally distinct actin filaments. *J Cell Sci* **128**: 2009–2019.

Gunning, P.W., Hardeman, E.C., Lappalainen, P., and Mulvihill, D.P. (2015b) Tropomyosin - master regulator of actin filament function in the cytoskeleton. *J Cell Sci* **128**: 2965–2974 https://jcs.biologists.org/content/128/16/2965.

Hai, C.M., and Murphy, R.A. (1989) Ca2+, crossbridge phosphorylation, and contraction. *Annu Rev Physiol* **51**: 285–298 https://pubmed.ncbi.nlm.nih.gov/2653183/.

Hanson, J., and Huxley, H.E. (1953) Structural basis of the cross-striations in muscle. *Nature* **172**: 530–532 https://www.nature.com/articles/172530b0.

Heling, L.W.H.J., Geeves, M.A., and Kad, N.M. (2020) MyBP-C: one protein to govern them all. *J Muscle Res Cell Motil* **41**: 91–101 https://www.ncbi.nlm.nih.gov/pmc/articles/PMC7109175/.

Herzberg, O., Moult, J., and James, M.N.G. (1987) CONFORMATIONAL FLEXIBILITY OF TROPONIN C11. In *Calcium-Binding Proteins in Health and Disease*. Elsevier, pp. 312–322 https://linkinghub.elsevier.com/retrieve/pii/B9780125210409500577.

Hitchcock-DeGregori, S.E., and An, Y. (1996) Integral repeats and a continuous coiled coil are required for binding of striated muscle tropomyosin to the regulated actin filament. *J Biol Chem* **271**: 3600–3603.

Hitchcock-DeGregori, S.E., and Singh, A. (2010) What makes tropomyosin an actin binding protein? A perspective. *J Struct Biol* **170**: 319–324 /pmc/articles/PMC2856766/?report=abstract.

Hitchcock-DeGregori, S.E., Song, Y., and Moraczewska, J. (2001) Importance of Internal Regions and the Overall Length of Tropomyosin for Actin Binding and Regulatory Function †. *Biochemistry* **40**: 2104–2112 https://pubs.acs.org/doi/10.1021/bi002421z.

Holmes, K.C. (1997) The swinging lever-arm hypothesis of muscle contraction. *Curr Biol* **7**: 112–118.

Holtzer, A., and Lowey, S. (1959) The Molecular Weight, Size and Shape of the Myosin Molecule. *J Am Chem Soc* **81**: 1370–1377 https://pubs.acs.org/doi/abs/10.1021/ja01515a026.

Homsher, E., Kim, B., Bobkova, A., and Tobacman, L.S. (1996) Calcium regulation of thin filament movement in an in vitro motility assay. *Biophys J* **70**: 1881–1892.

Huxley, A.F., and Niedergerke, R. (1954) Structural changes in muscle during contraction: Interference microscopy of living muscle fibres. *Nature* **173**: 971–973 https://www.nature.com/articles/173971a0.

Huxley, H., and Hanson, J. (1954) Changes in the Cross-striations of muscle during contraction and stretch and their structural interpretation. *Nature* **173**: 973–976 https://www.nature.com/articles/173973a0.

Inchingolo, A. V, Mihailescu, M., Hongsheng, D., and Kad, N.M. (2018) Single molecule imaging reveals the concerted release of myosin from regulated thin filaments. *bioRxiv* https://doi.org/10.1101/357202.

Inchingolo, A. V, Previs, S.B., Previs, M.J., Warshaw, D.M., and Kad, N.M. (2019) Revealing the mechanism of how cardiac myosin-binding protein C N-terminal fragments sensitize thin filaments for myosin binding. *Proc Natl Acad Sci U S A* **116**: 6828–6835 http://www.ncbi.nlm.nih.gov/pubmed/30877248.

Irving, M. (2017) Regulation of Contraction by the Thick Filaments in Skeletal Muscle. *Biophys J* **113**: 2579–2594.

Irving, M., Lombardi, V., Piazzesi, G., and Ferenczi, M.A. (1992) Myosin head movements are synchronous with the elementary force-generating process in muscle. *Nature* **357**: 156–158.

Jaqaman, K., Loerke, D., Mettlen, M., Kuwata, H., Grinstein, S., Schmid, S.L., and Danuser, G. (2008) Robust single-particle tracking in live-cell time-lapse sequences. *Nat Methods* **5**: 695–702 /pmc/articles/PMC2747604/?report=abstract.

Johnston, K., Jinha, A., and Herzog, W. (2016) The role of sarcomere length non-uniformities in residual force enhancement of skeletal muscle myofibrils. *R Soc Open Sci* **3** http://dx.doi.org/10.1098/rsos.150657orviahttp://rsos.royalsocietypublishing.org.

Karatzaferi, C., Chinn, M.K., and Cooke, R. (2004) The force exerted by a muscle cross-bridge depends directly on the strength of the actomyosin bond. *Biophys J* **87**: 2532–2544 /pmc/articles/PMC1304672/?report=abstract.

Kiani, F.A., Lehman, W., Fischer, S., and Rynkiewicz, M.J. (2019) Spontaneous transitions of actin-bound tropomyosin toward blocked and closed states. *J Gen Physiol* **151**: 4–8 /pmc/articles/PMC6314389/?report=abstract.

Kuo, I.Y., and Ehrlich, B.E. (2015) Signaling in muscle contraction. *Cold Spring Harb Perspect Biol* **7**: a006023 https://www.ncbi.nlm.nih.gov/pmc/articles/PMC4315934/.

Lehman, W., Galińska-Rakoczy, A., Hatch, V., Tobacman, L.S., and Craig, R. (2009) Structural Basis for the Activation of Muscle Contraction by Troponin and Tropomyosin. *J Mol Biol* **388**: 673–681 /pmc/articles/PMC2693027/?report=abstract.

Lehman, W., Rynkiewicz, M.J., and Moore, J.R. (2020) A new twist on tropomyosin binding to actin filaments: perspectives on thin filament function, assembly and biomechanics. *J Muscle Res Cell Motil* **41**: 23–38 https://doi.org/10.1007/s10974-019-09501-5.

Li, X. (Edward), Holmes, K.C., Lehman, W., Jung, H.S., and Fischer, S. (2010a) The Shape and Flexibility of Tropomyosin Coiled Coils: Implications for Actin Filament Assembly and Regulation. *J Mol Biol* **395**: 327–339 https://linkinghub.elsevier.com/retrieve/pii/S0022283609013199.

Li, X., Lehman, W., Fischer, S., and Holmes, K.C. (2010b) Curvature variation along the tropomyosin molecule. *J Struct Biol* **170**: 307–312.

Li, X.E., Suphamungmee, W., Janco, M., Geeves, M.A., Marston, S.B., Fischer, S., and Lehman, W. (2012) The flexibility of two tropomyosin mutants, D175N and E180G, that cause hypertrophic cardiomyopathy. *Biochem Biophys Res Commun* **424**: 493–496 /pmc/articles/PMC3412897/?report=abstract. Accessed September 28, 2020.

Longyear, T., Walcott, S., and Debold, E.P. (2017) The molecular basis of thin filament activation: From single molecule to muscle. *Sci Rep* **7**: 1822 http://www.ncbi.nlm.nih.gov/pubmed/28500282.

Lymn, R.W., and Taylor, E.W. (1971) Mechanism of Adenosine Triphosphate Hydrolysis by Actomyosin. *Biochemistry* **10**: 4617–4624 https://pubs.acs.org/doi/pdf/10.1021/bi00801a004.

Margossian, S.S., and Lowey, S. (1982) Preparation of Myosin and Its Subfragments from Rabbit Skeletal Muscle. *Methods Enzymol* **85**: 55–71 https://linkinghub.elsevier.com/retrieve/pii/007668798285009X.

Marques, M. de A., and Oliveira, G.A.P. de (2016) Cardiac troponin and tropomyosin: Structural and cellular perspectives to unveil the hypertrophic cardiomyopathy phenotype. *Front Physiol* **7**: 429 www.frontiersin.org.

Maytum, R., Lehrer, S.S., and Geeves, M.A. (1999) Cooperativity and switching within the three-state model of muscle regulation. *Biochemistry* **38**: 1102–1110.

McKillop, D.F., and Geeves, M.A. (1993) Regulation of the interaction between actin and myosin subfragment 1: evidence for three states of the thin filament. *Biophys J* **65**: 693–701 https://pubmed.ncbi.nlm.nih.gov/8218897/.

Ng, S.Y., Gunning, P., Eddy, R., Ponte, P., Leavitt, J., Shows, T., and Kedes, L. (1985) Evolution of the functional human beta-actin gene and its multi-pseudogene family: conservation of noncoding regions and chromosomal dispersion of pseudogenes. *Mol Cell Biol* **5**: 2720–2732.

Ohtsuki, I., and Morimoto, S. (2013) Troponin. In *Encyclopedia of Biological Chemistry: Second Edition*. Elsevier Inc., pp. 445–449 https://linkinghub.elsevier.com/retrieve/pii/B978012378630200195X.

Ooi, T., Mihashi, K., and Kobayashi, H. (1962) On the polymerization of tropomyosin. *Arch Biochem Biophys* **98**: 1–11 https://linkinghub.elsevier.com/retrieve/pii/0003986162901388.

Paulucci, A.A., Katsuyama, A.M., Sousa, A.D., and Farah, C.S. (2004) A specific C-terminal deletion in tropomyosin results in a stronger head-to-tail interaction and increased polymerization. *Eur J Biochem* **271**: 589–600 http://doi.wiley.com/10.1111/j.1432-1033.2003.03961.x.

Periasamy, M., Bhupathy, P., and Babu, G.J. (2008) Regulation of sarcoplasmic reticulum Ca2+ ATPase pump expression and its relevance to cardiac muscle physiology and pathology. *Cardiovasc Res* **77**: 265–273

https://academic.oup.com/cardiovascres/article/77/2/265/429379.

Perry, S. V (1998) Troponin T: Genetics, properties and function. *J Muscle Res Cell Motil* **19**: 575–602.

Perry, S. V (1999) Troponin I: Inhibitor or facilitator. .

Phillips, G.N., and Chacko, S. (1996) Mechanical properties of tropomyosin and implications for muscle regulation. *Biopolymers* **38**: 89–95.

Ratti, J., Rostkova, E., Gautel, M., and Pfuhl, M. (2011) Structure and interactions of myosin-binding protein C domain C0: Cardiac-specific regulation of myosin at its neck? *J Biol Chem* **286**: 12650–12658 https://pubmed.ncbi.nlm.nih.gov/21297165/.

Schevzov, G., Curthoys, N.M., Gunning, P.W., and Fath, T. (2012) Functional Diversity of Actin Cytoskeleton in Neurons and its Regulation by Tropomyosin. In *International Review of Cell and Molecular Biology*. Elsevier Inc., pp. 33–94 https://linkinghub.elsevier.com/retrieve/pii/B978012394309500002X.

Sousa, D., Cammarato, A., Jang, K., Graceffa, P., Tobacman, L.S., Li, X., and Lehman, W. (2010) Electron microscopy and persistence length analysis of semi-rigid smooth muscle tropomyosin strands. *Biophys J* **99**: 862–868 /pmc/articles/PMC2913205/?report=abstract.

Springall, L., Inchingolo, A. V., and Kad, N.M. (2016) DNA-protein interactions studied directly using single molecule fluorescence imaging of quantum dot tagged proteins moving on DNA tightropes. In *Methods in Molecular Biology*. Humana Press Inc., pp. 141–150 https://link-springer-com.chain.kent.ac.uk/protocol/10.1007/978-1-4939-3631-1_11.

Sweeney, H.L., and Hammers, D.W. (2018) Muscle contraction. *Cold Spring Harb Perspect Biol* **10** /pmc/articles/PMC5793755/.

Swenson, C.A., and Stellwagen, N.C. (1989) Flexibility of smooth and skletal tropomyosins. *Biopolymers* **28**: 955–963 http://doi.wiley.com/10.1002/bip.360280504.

Szczesna-Cordary, D., Jones, M., Moore, J.R., Watt, J., Kerrick, W.G.L., Xu, Y., *et al.* (2007) Myosin regulatory light chain E22K mutation results in decreased cardiac intracellular calcium and force transients. *FASEB J* **21**: 3974–3985 https://onlinelibrary.wiley.com/doi/abs/10.1096/fj.07-8630com.

Szent-Györgyi, A.G. (1975) Calcium regulation of muscle contraction. *Biophys J* **15**: 707–723 https://linkinghub.elsevier.com/retrieve/pii/S0006349575858498.

Takeda, S. (2005) Crystal structure of troponin and the molecular mechanism of muscle regulation. In *Journal of Electron Microscopy*. pp. i35–i41 http://academic.oup.com/jmicro/article/54/suppl_1/i35/984885/Crystal-structure-of-troponin-and-the-molecular.

Tardiff, J.C. (2005) Sarcomeric proteins and Familial Hypertrophic Cardiomyopathy: Linking mutations in structural proteins to complex cardiovascular phenotypes. *Heart Fail Rev* **10**: 237–248 https://pubmed.ncbi.nlm.nih.gov/16416046/.

Tinevez, J.Y., Perry, N., Schindelin, J., Hoopes, G.M., Reynolds, G.D., Laplantine, E., *et al.* (2017) TrackMate: An open and extensible platform for single-particle tracking. *Methods* **115**: 80–90.

Tobacman, L.S. (1996) Thin filament-mediated regulation of cardiac contraction. *Annu Rev Physiol* **58**: 447–481 www.annualreviews.org.

Uyeda, T.Q.P., Kron, S.J., and Spudich, J.A. (1990) Myosin step size. Estimation from slow sliding movement of actin over low densities of heavy meromyosin. *J Mol Biol* **214**: 699–710.

Vedula, P., and Kashina, A. (2018) The makings of the “actin code”: regulation of actin’s biological function at the amino acid and nucleotide level. *J Cell Sci* **131**: jcs215509 https://journals.biologists.com/jcs/article/131/9/jcs215509/57120/The-makings-of-the-actin-code-regulation-of-actin.

Vibert, P., Craig, R., and Lehman, W. (1997) Steric-model for activation of muscle thin filaments 1 1 Edited by P.E. Wright. *J Mol Biol* **266**: 8–14 https://linkinghub.elsevier.com/retrieve/pii/S0022283696908001.

Wang, C., Schwan, J., and Campbell, S.G. (2016) Slowing of contractile kinetics by myosin-binding protein C can be explained by its cooperative binding to the thin filament. *J Mol Cell Cardiol* **96**: 2–10 https://pubmed.ncbi.nlm.nih.gov/26454159/.

Wegner, A., and Isenberg, G. (1983) 12-fold difference between the critical monomer concentrations of the two ends of actin filaments in physiological salt conditions. *Proc Natl Acad Sci U S A* **80**: 4922–4925 https://pubmed.ncbi.nlm.nih.gov/6576365/.

Yang, S., Barbu-Tudoran, L., Orzechowski, M., Craig, R., Trinick, J., White, H., and Lehman, W. (2014) Three-dimensional organization of troponin on cardiac muscle thin filaments in the relaxed state. *Biophys J* **106**: 855–864 /pmc/articles/PMC3944806/?report=abstract.

Zhu, L., Zhang, Y., Hu, Y., Wen, T., and Wang, Q. (2013) Dynamic actin gene family evolution in primates. *Biomed Res Int* **2013** /pmc/articles/PMC3690210/?report=abstract.